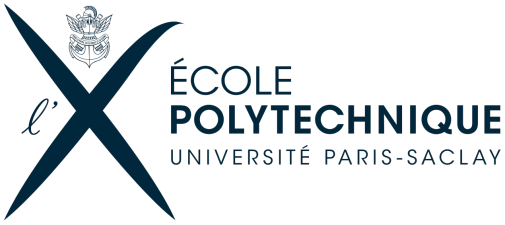

ÉCOLE POLYTECHNIQUE
MASTER PHYSIQUE DES HAUTES ÉNERGIES
GÖTZ Niklas

RAPPORT DE STAGE DE RECHERCHE

Kinetic theory for momentum-dependent scattering

RAPPORT NON CONFIDENTIEL

Département de physique
PHY 591 : Champs, particules et matière
Enseignant référent : Stephane MUNIER
Tuteur de stage dans l'organisme : François GELIS
Dates du stage : 01 Avril 2019 - 31 juilliet 2019
Adresse de l'organisme :
Institut de Physique Théorique
Orme des Merisiers bâtiment 774
Point courrier 136
CEA/DSM/IPhT, CEA/Saclay
F-91191 Gif-sur-Yvette Cedex

Déclaration d'intégrité relative au plagiat

Je soussigné Götz, Niklas certifie sur l'honneur :

1. Que les résultats décrits dans ce rapport sont l'aboutissement de mon travail.
2. Que je suis l'auteur de ce rapport.
3. Que je n'ai pas utilisé des sources ou résultats tiers sans clairement les citer et les référencer selon les règles bibliographiques préconisées.

Mention à recopier

Je déclare que ce travail ne peut être suspecté de plagiat.

Date 11.7.19 Signature

Kinetic theory for momentum-dependent scattering

GÖTZ Niklas

Résumé

À partir du cadre de la théorie du champ effectif *Color Glass Condensate*, il est présenté comment obtenir une description des collisions d'ions lourds dans un montage de théorie cinétique afin d'étudier le processus de thermalisation de l'état de la matière dense gluonique vers un état d'équilibre. En cela, l'équation de Boltzmann avec des interactions scalaires élastiques de type point peut être généralisée pour inclure la condensation de Bose-Einstein. Il est présenté comment améliorer cette approche numérique afin de prendre également en compte les amplitudes de diffusion dépendant de la quantité de mouvement sans avoir à résoudre les intégrales complètes à cinq dimensions. Cela permet d'analyser le comportement des premiers états après la collision dans des conditions plus réalistes. De nombreux exemples d'applications de cette amélioration sont donnés, permettant de mieux comprendre l'influence de différentes plages de quantité de mouvement sur le processus de condensation, l'importance de la masse de tamisage pendant les premiers temps de l'évolution et l'effet de l'amplitude de diffusion sur la vitesse de thermalisation. Plusieurs propositions d'améliorations supplémentaires sont présentées.

Abstract

Starting from the Color Glass Condensate effective field theory framework, it is presented how to reach a description of heavy ion collisions in a kinetic theory setup in order to investigate the thermalization process of the dense gluonic matter state towards an equilibrium state. In this, the Boltzmann equation with elastic point-like scalar interactions can be generalised to include Bose-Einstein-condensation. It is presented how to improve this numerical approach in order to also consider momentum-dependent scattering amplitudes without having to solve the full five-dimensional integrals. This allows to analyse the behaviour of the early states after the collision under more realistic conditions. Multiple examples for applications of this improvement are given, leading to insights about the influence of different momentum ranges on the condensation process, the importance of the screening mass for early times of the evolution and the effect of the scattering amplitude on the thermalization speed. Several proposals for further improvements are given.

Contents

Introduction

The “strong interaction” is special due to its non-perturbative and non-linear nature. As a consequence, quarks and gluons as well as any colored excitations in general cannot be detected directly by experiments, as they must be confined into color-singlets, such as mesons or baryons. For high temperatures however, fundamental degrees of freedom should be accessible due to the asymptotic freedom of Quantum Chromodynamics (QCD), the gauge theory of the strong interaction. They allow to probe properties of hot and dense matter with manifested quarks and gluons for high energies. This is realised with modern heavy-nuclei colliders. Such collisions pose a challenge to the theoretical description in QCD, as hard short distance processes as well as non-perturbative long distance soft physics are involved. This motivated the collection of experimental data.

During the past years, ultra-relativistic heavy ion collisions both a the RHIC in BNL and at the LHC in CERN have accumulated a great amount of information on properties of strongly interacting quark-gluon matter in QCD. In this process, a Quark Gluon Plasma (QGP) consisting of quasi-free quarks and gluons is formed, which is a nearly thermal state and experiences hydrodynamic expansion [1]. It represents a testing ground for the Standard Model, as well as for finite temperature field theory and possible grand unification theories. It is also of cosmological significance, as the early universe (around a age of 10 microseconds and a temperature higher than 150 MeV) was dominated by this phase of matter [2]. The QGP expands in a viscous-hydrodynamic way and eventually cools down enough to hadronize into the hadronic gas that further expands and ultimately cools down further into individual hadrons, which are finally measured by detectors. However, it has been proven to be challenging to understand the thermalization mechanism that leads to the QGP forming from a dense gluonic matter state, nicknamed "Glasma", on the basis of the first principles of QCD, as there is an interplay of several overlapping time scales. This Glasma is a short-lived state, described by purely longitudinal strong color fields.

As mentioned hydrodynamics has been shown to be an excellent phenomenological description of the processes leading to hadronization and requires rapid thermalization at a timescale below 1 fm/c ([1, 3]), implying strong interactions, which is in conflict with the high momentum scale of the initial state. The typical momenta of the nuclei are of the saturation scale Q_S, which grows with beam energy and the size of the used nuclei. Because it is the only relevant time scale in the problem, the

formation time of gluons after the collision is of order $1/Q_S$ [4]. A perturbative QCD approach implies that the following thermalization time (and by this the time of onset of hydrodynamical behaviour) is of order $\alpha_S^{-\frac{13}{5}} Q_S^{-1}$ for Q_S being large compared to the QCD-scale Λ_{QCD} [5]. For the experiments done at RHIC, Q_S is about 1 - 2 GeV, which leads to an estimate of thermalization time of several fm/c for a coupling of order one, which is the case for this perturbative approach as one uses very high energies or very large nuclei. This clearly shows that this so called "bottom up" approach is not satisfying as it is not in agreement with the RHIC data and a non-perturbative approach is needed. It is still in question if the perturbative approach is able to describe thermalization at all [6], as the bulk of particle production processes is of low momentum and the characteristic momenta decrease with time due to the expansion. Even the hard scale interactions are not necessarily perturbative in the sense of loop expansion, as often resummations are required. Therefore, other candidates for an early thermalization mechanism have to be considered, such as approaches based on AdS/CFT correspondence, where the thermalization appears as a formation of a black hole horizon in the dual theory [7–10].

Other ways to investigate the thermalization are built up on he framework of Color Glass Condensate (CGC) effective theory [11], in which the evolution of the gluon fields in leading order of the strong coupling constant g^2 behaves like the collision of coherent classical Yang–Mills fields [12]. The CGC describes the initial condition before and at the time of the collision, as well as the short time after the collision. It approximates the description of the fast partons in the wave function of a hadron by using the fact that their dynamics is slowed down by relativistic effects, and provides a way to track the evolution of states with energies that are relevant in the dense regime. In the McLerran-Venugopalan model (CGC at lowest order, with a local Gaussian distribution of color source) description, the Glasma does not show the required behaviour [13]. At this order, the energy-momentum tensor has a negative longitudinal pressure, and by this does not agree with the hydrodynamical description of the expansion and never isotropizes. It is therefore necessary to go beyond lowest order. During this, a resummation process becomes necessary. Instabilities similar to plasma instabilities occur here, of which the origin is not clear yet ([13, 14]). They play a key role of higher orders during the resummation process. There are multiple approaches of performing the resummation in form of a numerical approximation. One is based on the Boltzmann equation in the context of kinetic theory from the Dyson-Schwinger equations. In the regime of large occupation numbers, classical field theory and kinetic theory essentially describe the same dynamics [15]. The collision term is expressed in terms of self-energies in the Schwinger-Keldysh formalism and allows to assess the behaviour of the underlying quantum field theory. This can be then solved numerically. This approach has been proven to be a much less costly of investigating the process of thermalization than other approximations, like the Classical Statistical Approximation (CSA) [16]. Additionally, it helps to gain an intuitive understanding from its connection to statistical physics.

A Boltzmann solver for a elastic, isotropic and spatially homogeneous ϕ^4 interaction for the CGC was presented in [17], on which this work is based. There, solving the Boltzmann equation numerically in an efficient way required the reduction of a 5- into a 2-dimensional integral, for which strict assumptions had to be made. An alternative way to do this is a desirable goal, in order to

cover a greater amount of cases, opening the way to include more realistic scattering amplitudes into the simulation and by this to study more relevant processes. This will be the central task of this work.

Chapter 1 reviews the derivation of the CGC, starting by describing the kinematics of heavy ion collisions and describing the need of resummation for NLO observables. It is demonstrated how the problem of thermalization arises in the context of the CGC, inspired by [18]. Chapter 2 outlines the derivation of the Boltzmann equation in the context of kinetic theory, especially the generalisation of including the possibility of forming a Bose-Einstein condensate. This is necessary as heavy-ion-collisions produce overoccupied initial conditions. Chapter 3 summarises the work done in [17], starting by explaining the general setup of the simulation as well as discussing important questions about the right discretization and methods to ensure a constantly high accuracy of the calculations. In a second step, chapter 3 demonstrates the original and the new alternative way of calculating the collision kernel and by this allowing more realistic simulations in exchange for slightly higher computational costs. It is explained how to restore the Mandelstam variables during the calculation. Chapter 4 presents applications of the improved simulation, and their implications to the problem of thermalization, which give several insights especially about the crucial role of the screening mass, the role of different momentum ranges on the condensate evolution (and by this on the whole thermalization process) as well as on the speed of thermalization.

Chapter 1

The Color Glass Condensate

1.1 Heavy nuclei at high energy

CGC is an effective field theory, that means, an approximate description of the underlying quantum field theory for a specific energy range. This leads to a reduction of parameters (by integrating them out or using symmetries) and by this simplifies the description of the model, which is especially interesting for underlying theories which are otherwise hard to treat. On the other hand, it limits the situations where the theory can be applied. In the case of CGC, one is restricted to collisions between heavy hadrons/nuclei at very high energy. The advantage of a high energy collision is that, due to the time dilation, the interactions between the otherwise complicated internal dynamics of the hadron are absorbed in the change of the parton distribution, which legitimates the assumption of the parton model of quasi-free particles. High energy alone is not a sufficient condition for the application of the CGC. To be more precise, CGC describes the hadron in the saturation regime, which will be outlined in the following.

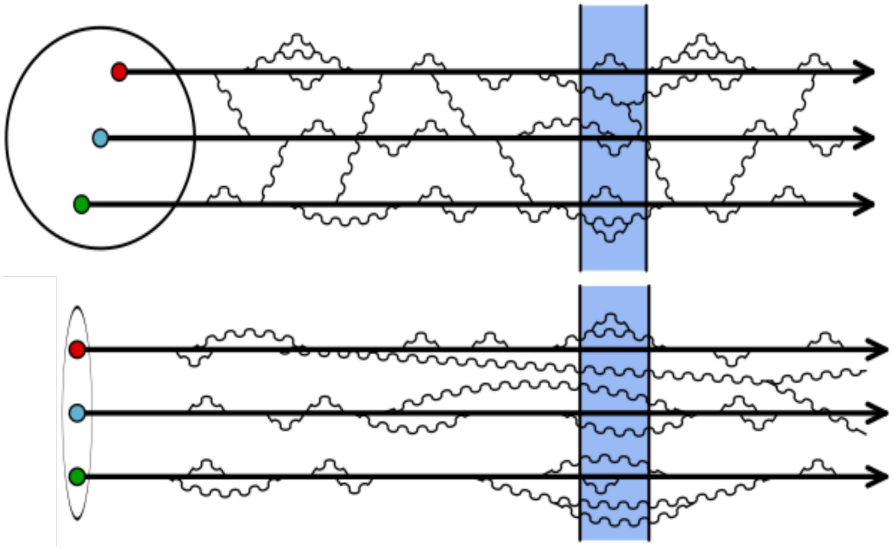

Figure 1.1 – Sketch of fluctuations inside a nucleon. Top: slow nucleon. Bottom: boosted nucleon. Due to the Lorentz time dilatation, virtual fluctuations become "on-shell". From [18].

The hadrons consist of three valence quarks, which interact by short lived fluctuating virtual quarks and gluons. As long as the lifetime of the virtual particles is smaller than the characteristic timescale of the probe, they only modify the parameters of the Lagrangian by renormalization. Long-lived fluctuations are, on the other hand, seen as partons which are on-shell (in a definition of on-shellness which is relaxed by the uncertainty principle), as it is displayed in Figure 1.1. As the collision time scales as the inverse collision energy, the parton distribution grows with the collision energy, as more and more virtual particles have a relatively long lifetime. During a measurement of a process with transverse momentum Q, a fixed distance of order Q^{-1} is resolved. Particles which are seen as non-virtual in this probe had then the spatial extension of their wave function inside this space. If one increases the collision energy, the number of partons increases and they fill all the available space in the hadron. The density of gluons becomes high enough for interactions between gluons to be dominant, which is called gluon saturation. The gluon occupation number is limited by α_s^{-1}, the point at which splittings and recombinations balance. In deep inelastic scattering experiments, a condition for gluon saturation via the transverse momentum was found as $Q^2 < Q_S^2 \sim x^{-0.32}$ [19] with the Bjorken-x, which is small at high energy. A more useful threshold for gluon saturation and by this for the application of CGC is given by looking at the point from which gluon recombinations becomes likely, which is when the product of the recombination cross section $\alpha_S Q^{-2}$ and the surface density of gluons $A^{-2/3} x G(x, Q^2)$ (A is the mass number, G the gluon density) becomes larger than one. This means that the partons, which emit gluons and form by this cascades, start to interact by recombining gluons. This causes non-linearities in the gluon distribution. One sees also

$$Q^2 \leq Q_S^2 \equiv \frac{\alpha_s x G(x, Q_S^2)}{A^{2/3}}. \tag{1.1}$$

As long as a process has a smaller typical momentum scale than Q_S, it is dominated by saturation. As the gluon distribution is proportional to the nucleon volume [20], one gets together with the observation about the proportionality of the momentum fraction the relation $Q_S^2 \sim A^{1/3} x^{-0.32}$. Therefore, there is a window between this scale and Λ_{QCD} (below which confinement dominates), which grows with the size of the nuclei as well as with decreasing x, in other words rising energies. Q_S ranges between 1.2 GeV for the RHIC and 2 GeV for the LHC [20].

For a system in which the observer is at rest and the hadron has a very high momentum, one uses the convenient light cone coordinates

$$x^+ \equiv \frac{x^0 + x^3}{\sqrt{2}}, \quad x^- = \frac{x^0 - x^3}{\sqrt{2}}. \tag{1.2}$$

The direction of motion is x^3. This definition may also be applied to the momentum. A boost in z-direction results in a scaling with e^ω for x^+. Partons having a high longitudinal momentum are slowed down by relativistic effects and appear to be static in the transverse plane. As the evolution of x^+ is determined by p^- and this is going to zero for massless case due to $p^- = \mathbf{p}_T^2/(2p^+)$, the color current being the only relevant information about fast partons becomes

$$J_a^\mu \equiv \delta^{\mu+} \rho_a(x^-, \boldsymbol{x}_T) \tag{1.3}$$

with the spatial distribution of color charge ρ_a. One expects a peak around $x^- = 0$ due to Lorentz contraction, but an undetermined distribution in the transverse plane. The color distribution is there-

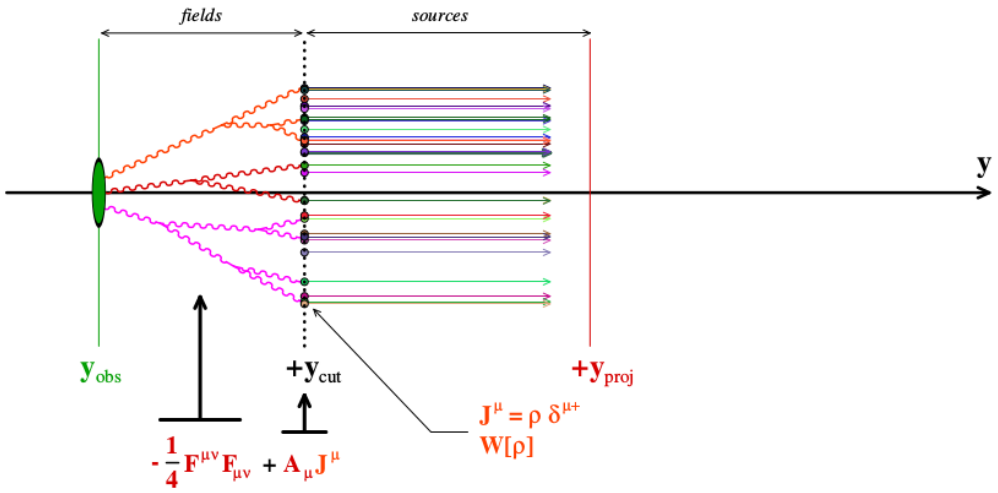

Figure 1.2 – Degrees of freedom in the CGC effective description of a high energy hadron. From [18].

fore unknown and can be seen as a random variable with probability distribution $W[\rho]$. Therefore, the expectation value of an observable becomes the functional average

$$\langle \mathcal{O} \rangle = \int [\mathrm{D}\,\rho] W[\rho] \mathcal{O}[\rho]. \tag{1.4}$$

1.2 LO approximation

To calculate this, one has to determine the observable for an arbitrary configuration of the color charge density and then perform the weighted average. However, it is not clear at this point if the two densities of the two nuclei are dependent of each other. This is crucial for being able to use this factorisation and will become clearer soon.

This description has of course its limitations. For any parton with too small rapidity in the observer frame, the approximations will fail. Therefore a cutoff rapidity between the observer and the hadron rapidity has to be introduced. Partons with a lower rapidity will be described as gauge fields, that means according to the original Yang-Mills-action, such with higher rapidity will be approximated as outlined above . This, together with the assumptions of a nearly Gaussian probability distribution, leads to what is called the McLerran-Venugopalan model, which is basically the Color Glass Condensate at lowest order [21–23].

Figure 1.2 displays the approximation of degrees of freedom . The action has therefore two contributions, the Yang-Mills and an eikonal contribution, and reads

$$\mathcal{S}_{CGC} = \int d^4x \left(-\frac{1}{4} F_{\mu\nu} F^{\mu\nu} + J^\mu A_\mu \right) \tag{1.5}$$

Next, one can take a look on the power counting in the saturation regime. This refers to a gluon occupation number of g^{-2}, as at this point recombinations and splittings of gluons balance each other. As the occupation number is quadratic in the gauge fields, of which ρ is the density, it follows

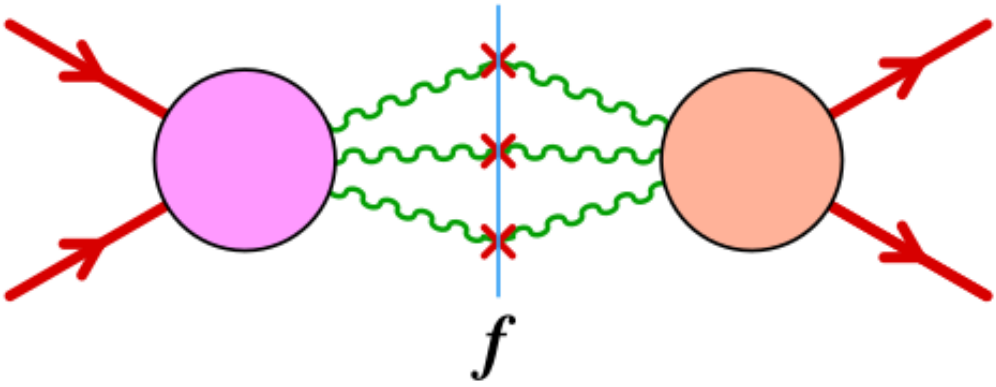

Figure 1.3 – Illustration of the Schwinger-Keldysh formalism. The final state is in the centre, the right side is the complex-conjugate of the left side. From [18].

$\rho \sim g^{-1}$, and the same is true for the color current by construction. One has by this strong sources in a dense regime and can use the results of [24] for the power counting of connected graphs in the CGC (for disconnected diagrams, it can be applied to the subdiagrams). The calculation is equally valid for quartic or other vertices. The order of each graph therefore reads

$$\mathcal{G} \sim g^{-2} g^{n_E} g^{2n_L} \tag{1.6}$$

with the number of external gluons n_E and loops n_L. As the observables depend now non-pertubatively of the number of sources, they are at tree level given by an infinite sum of tree diagrams with arbitrary many insertions of the current.

In practise, one wants to work most of the time with inclusive observables, that means quantities which are averaged over all final states. The following results are only valid for such observables, as exclusive quantities show a difficult behaviour [18]. It is also assumed that the initial state only contains the two nuclei, which can be absorbed in the source term. In order to calculate the inclusive observables, it is favourable to use the Schwinger-Keldysh formalism ([25, 26]), also known as closed time path formalism. This is similar to Cutkosky's cutting rules [27] and includes all the necessary steps to compute

$$\langle \mathcal{O} \rangle = \sum_{\text{final states } f} P(AA \to f) \mathcal{O}[f]. \tag{1.7}$$

This is achieved by expanding the time integration to a path which covers the full timeline both in the conventional ordered sense and the inversed one. The generating functional is connected to the conventional of time-ordered perturbation theory, which can be proven using the fact that interactions are always trivially factorizable:

$$Z[j_+, j_-] = \exp\left[\int dx^4 dy^4 \Box_x \Box_y G^0_{+-}(x,y) \frac{\delta^2}{\delta j_+(x) \delta j_-(y)} \right] Z[j_+] Z^*[j_-] \tag{1.8}$$

One has additionally the massless propagators

$$G^0_{+-} = 2\pi\theta(-p^0)\theta(p^2), \quad G^0_{++}(p) = \frac{i}{p^2 + i\epsilon}, \quad G^0_{--}(p) = \frac{-i}{p^2 + i\epsilon}. \tag{1.9}$$

The first one is used for the on-shell particles on the line of the final state, whereas the other two are used for the internal lines left and right in figure 1.3, in other words, for the normal and the

complex-conjugate amplitude. One says that G^0_{+-} "stitches" ordinary perturbation theory and its complex-conjugate counterpart. In this framework, one calculates the inclusive observable in the following way:

— One draws all $AA \to AA$ diagrams at a given order in g^2, with the power counting as seen before.

— One sums over all possible assignments of + and - on the internal vertices, which are connected by the respective propagators.

— One sets all unconnected graphs to zero, and integrates over the real axis.

The simplification arises as one can always use these relations to get a retarded propagator, which replaces the sum over the + and - indices:

$$G_{++} + G_{--} = G_{+-} + G_{-+} \tag{1.10}$$

$$G_{++} - G_{+-} = G_{-+} - G_{--} = G_R \tag{1.11}$$

This leads in leading order to an infinite sum of tree diagrams built with retarded propagators (due to the sum over all + and - indices) and an arbitrary number of current insertions, as they do not change the power counting. However, all of this graphs are structured recursively, therefore the sum can be seen as Green's formula for an initial surface at $-\infty$. This can be expressed by the classical solutions of the Yang-Mills equations with vanishing retarded boundary conditions

$$[D_\mu, F^{\mu\nu}]_a = \rho_1 \delta^{\nu+} + \rho_2 \delta^{\nu-}, \quad \lim_{x^0 \to -\infty} A^\mu(x) = 0. \tag{1.12}$$

It is now sufficient to solve these equations, which enables to express the solution in A^μ.

1.3 Cutoff-dependence at higher orders

In a next step, one can take a look on the NLO, which is given by the sum of all 1-loop diagrams, which are of order $\mathcal{O}(1)$ in the coupling constant. However, one has to be aware of the cutoff y_{cut} introduced earlier. When integrating over the loop, one has to respect it, as one otherwise enters the domain of static sources and by this double-counts these terms. Therefore, the loop diagrams can be dependent on the cutoff [28], and a n-loop diagram can have a dependency up to order n. The terms with maximum order of dependence of the cutoff are called leading log terms, as the cutoff is usually defined as being the logarithm of a cutoff on the longitudinal momentum. However, as the cutoff is arbitrary, the observables should not depend on it. The aim is to absorb the leading log dependency in a redefinition of the probability distribution in 1.4, which turns it into a cutoff-dependent object. Note that although $W[\rho]$ will be then cutoff dependent, it has always the same dependency and may be used for all inclusive observables.

In order to achieve this, one can use a relationship between the LO and NLO observable. This can be formally written as

$$\langle \mathcal{O}(\phi) \rangle_{\mathrm{NLO}} = \int d^3\boldsymbol{x} \delta\Phi(x) \frac{\delta \mathcal{O}(\Phi)}{\delta \Phi(x)} + \frac{1}{2} \int d^3\boldsymbol{x} d^3\boldsymbol{y} G(x,y) \frac{\delta^2 \mathcal{O}(\Phi)}{\delta\Phi(x)\delta\Phi(y)}. \tag{1.13}$$

It includes two corrections, a 1-loop correction to the classical field $\delta\Phi(x)$ and a propagator dressed by the background field Φ. All of the fields are separated by space-like intervals, as one looks at the

final state, so one does not need to differ between the subscripts + and -. It was shown in [29] that there exists the following relationship for all inclusive variables:

$$\mathcal{O}_{\mathrm{NLO}} = \left[\frac{1}{2}\int_{\boldsymbol{uv}} \boldsymbol{\Gamma}_2(\boldsymbol{u},\boldsymbol{v})\mathcal{T}_{\boldsymbol{u}}\mathcal{T}_{\boldsymbol{v}} + \int_{\boldsymbol{u}} \boldsymbol{\alpha}(\boldsymbol{u})\mathcal{T}_{\boldsymbol{u}}\right]\mathcal{O}_{\mathrm{LO}} \tag{1.14}$$

where $\mathcal{O}_{\mathrm{LO}}$ is seen as a functional of initial values on a hypersurface over which one integrates. $\mathcal{T}_{\boldsymbol{u}}$ shifts the initial field:

$$\exp\left[\int_{\boldsymbol{u}} \boldsymbol{\alpha}(\boldsymbol{u})\mathcal{T}_{\boldsymbol{u}}\right] F(A_{\mathrm{init}}) = F[A_{\mathrm{init}} + \boldsymbol{\alpha}] \tag{1.15}$$

The expression of $\boldsymbol{\Gamma}_2$ is:

$$\boldsymbol{\Gamma}_2(\boldsymbol{u},\boldsymbol{v}) = \int \frac{d^3\boldsymbol{k}}{(2\pi)^3 2\omega_{\boldsymbol{k}}} a_{\boldsymbol{k}}(\tau_0,\boldsymbol{u})a^*_{\boldsymbol{k}}(\tau_0,\boldsymbol{v}) \tag{1.16}$$

with τ_0 being the initial time and the $a_{\boldsymbol{k}}$ being small perturbations around the classical field, having color, spin and Lorentz indices being hidden here. Note that both $\boldsymbol{\Gamma}_2$ and $\boldsymbol{\alpha}$ in 1.14 are universal for all inclusive observables, but not valid for exclusive ones. As the operator in front of the LO observable only acts on the initial values, the time evolution at NLO stays classical, just like at LO. As the LO result depends only on the classical field, quantum effects in the evolution do only enter at orders higher than NLO. However, quantum corrections can still enter from the initial state, which is the effect of $\mathcal{T}_{\boldsymbol{u}}\mathcal{T}_{\boldsymbol{v}}$. It can be shown that this is a general property of quantum mechanics [18].
With this result, one can investigate the cutoff-dependence at NLO. [29] shows how to use this in order to obtain the cutoff dependence. An important relation for this procedure is , when keeping only terms linear in the cutoff [29]

$$\mathcal{O}_{\mathrm{NLO}} \underset{\mathrm{LLog}}{=} y^+_{cut} H_1 \mathcal{O}_{\mathrm{LO}}(A^+) + y^-_{cut} H_2 \mathcal{O}_{\mathrm{LO}}(A^-) \tag{1.17}$$

where one uses the JIMWLK Hamiltonian [30–33] for each of the nuclei

$$H = \frac{1}{2}\int_{\vec{\boldsymbol{x}}_T,\vec{\boldsymbol{y}}_T} \frac{\delta}{\delta\rho_a(\vec{\boldsymbol{x}}_T)}\chi_{ab}(\vec{\boldsymbol{x}}_T,\vec{\boldsymbol{y}}_T)\frac{\delta}{\delta\rho_a(\vec{\boldsymbol{y}}_T)} \tag{1.18}$$

with

$$\begin{aligned}\chi_{ab}(\vec{\boldsymbol{x}}_T,\vec{\boldsymbol{y}}_T) =& \frac{\alpha_S}{4\pi^3}\int d^2\vec{\boldsymbol{z}}_T \frac{(\vec{\boldsymbol{x}}_T-\vec{\boldsymbol{z}}_T)\cdot(\vec{\boldsymbol{y}}_T-\vec{\boldsymbol{z}}_T)}{(\vec{\boldsymbol{x}}_T-\vec{\boldsymbol{z}}_T)^2(\vec{\boldsymbol{y}}_T-\vec{\boldsymbol{z}}_T)^2} \\ &\times\left[\left(1-\tilde{U}^\dagger(\vec{\boldsymbol{x}}_T)\tilde{U}(\vec{\boldsymbol{z}}_T)\right)\left(1-\tilde{U}^\dagger(\vec{\boldsymbol{z}}_T)\tilde{U}(\vec{\boldsymbol{y}}_T)\right)\right]_{ab}\end{aligned} \tag{1.19}$$

where $\tilde{U}$ is a Wilson line in adjoint representation constructed form the gauge field A^+ such that $\nabla^2_T A^+ = -\rho$. "LLog" stands for leading log terms. These are terms in maximal degree of the cutoff. 1.17 is an expression for these terms which we intend to absorb in the probability distribution. The $+/-$ superscript at the cutoff stands for the right or left moving nucleus. One realises that 1.17 is a sum without a mixing term, so that the cutoff dependent term is an intrinsic property of the moving nucleus itself. With these definitions, one can also write

$$\frac{1}{2}\int_{\boldsymbol{uv}} \boldsymbol{\Gamma}_2(\boldsymbol{u},\boldsymbol{v})\mathcal{T}_{\boldsymbol{u}}\mathcal{T}_{\boldsymbol{v}} + \int_{\boldsymbol{u}} \boldsymbol{\alpha}(\boldsymbol{u})\mathcal{T}_{\boldsymbol{u}} = y^+_{cut}H_1 + y^-_{cut}H_2 \tag{1.20}$$

with one term for each nucleus. This allows us to redefine the source distributions of each nucleus and by this eliminate cutoff dependence.

This result follows also from a heuristic argument: Remembering that the cutoff was introduced in order to deal with the low-energy gluons being produced when boosting the nucleus up to gluon saturation, one sees that they have a very long formation time due to the uncertainty principle, longer than the time frame of collision. Therefore they had to exist before. As the nuclei have space-like separation until the point of collision, causality forces the cutoff-dependent terms to be unmixed.

One can now eliminate the cutoff-dependence by integrating over all possible color charge densities in the projectiles, as these are anyway unknown. Using the fact that the JIMWLK Hamiltonian is a self-adjoint operator, one can use

$$\int [D\rho] W(H\mathcal{O}) = \int [D\rho](HW)\mathcal{O} \tag{1.21}$$

which allows in the end to transfer in 1.4 for NLO the cutoff-dependence together with the action of the Hamiltonian into the probability distribution $W[\rho]$, using 1.14 and the approximation 1.17, such that $W[\rho] \to W[\rho] - y_{cut} H W[\rho]$. This would cancel the linear dependence on y_{cut}. This is connected to the equivalent approach for an infinitesimal variation δy_{cut}, which amounts to the JIMWLK equation

$$\frac{\partial W[\rho]}{\partial y_{cut}} = -HW[\rho] \tag{1.22}$$

which tells how the probability distribution varies with the cutoff. The same procedure is valid for any inclusive variable. By this, it is achieved that the leading log cutoff-dependency has been cancelled.

1.4 Thermalization in the CGC framework

With this tools, CGC can describe the earliest stages of a heavy ion collision. However, eventually, the hadronization will happen when the energy density falls below the critical QCD energy density. This has not been included in CGC. Nevertheless, there has to be an intersection between the regime of CGC and the hydrodynamic regime of hadronization. CGC should be able to produce an initial state from which on hydrodynamics can evolve the system further. It has been outlined in [18] that even if there is some success in matching at LO of CGC, this is not possible due to a non-fitting behaviour of the energy-momentum-tensor: The ration between longitudinal and transverse pressure remains much too slow to be in agreement with hydrodynamics. The same is true when resumming the leading log corrections, which is absorbed in the evolution of the distributions $W[\rho]$ [18].

A possible solution to this is an instability of the boost invariant solutions of the classical Yang-Mills equations ([13, 34, 35]). A small pertubation of the initial conditions, when being dependent of the rapidity, leads to a divergence of the perturbed relatively to the unperturbed. This is related to the Weibel instabilities of QED for anisotropic plasmas [36–38]. These instabilities are a great problem for the power counting which has been developed before, as this was only done by comparing orders of g^2. Now, time dependent factors can grow exponentially and cause higher order contributions to become greater than leading orders. This sets a limiting time scale at which the quantum fluctuations become as large as the initial background classic fields. Although this forces one to improve

the power counting, the effect of this instabilities is to map a compact support into a greater area of the phase-space than only at NLO, which greatly supports the thermalization process, as they lead to a very fast isotropization [39]. The plasma instabilities generically arise as a consequence of anisotropy and lead to exponential growth of modes that help restore the isotropy. Comparable to particle scatterings tend to randomize and thus isotropize the momentum distribution in a gas, the classical fields have interactions built in and it is not surprising that the fluctuations on top of the fields lead to a higher isotropy.

The perturbations in 1.16 grow due to the instabilities for certain values of $\boldsymbol{k}$ exponentially in time. By this, it compensates the factor of g^2 of the loop contribution (via $\mathcal{T}$) and can reach the same size as LO terms. Such a problem can occur at any loop order. Therefore, an alternative strategy has to be applied, in such a way that one only keeps the most important terms with respect to the instabilities, too. This is achieved by scaling the perturbation of the classical field in the expansion with a factor of order $\exp(\sqrt{\mu\tau})$, that means, adding this factor to $\mathcal{T}$. Here, μ is the order of Q_S and τ the time. The expansion of an observable becomes

$$\mathcal{O} = c_0 g^{-2} + c_1 g^0 e^{2\sqrt{\mu\tau}} + \dots . \tag{1.23}$$

At higher orders, not all terms have the same growth in time as for the 2-loops, for example, one can connect four or only three perturbed initial values by loops, which give the respective time-dependent factors. This affects the order of the time growth as well as how often this contribution is counted (which corresponds to symmetry factors). It can be shown that the right resummation is

$$\mathcal{O}_{\text{resummed}} = \exp\left[\frac{1}{2}\int_{\boldsymbol{uv}} \boldsymbol{\Gamma}_2(\boldsymbol{u},\boldsymbol{v})\mathcal{T}_{\boldsymbol{u}}\mathcal{T}_{\boldsymbol{v}}\right]\mathcal{O}_{\text{LO}}. \tag{1.24}$$

Note that only terms with second derivatives have been counted, as terms with only one derivative (e.g. having $\mathcal{T}$ only acting once) have a much slower growth with time. By this, one regains the results of LO and NLO as before, as well as a subset of higher loop contributions. Using the well known identity

$$e^{\frac{\alpha}{2}\partial_x^2} f(x) = \int_{-\infty}^{+\infty} dz \frac{e^{-z^2/2\alpha}}{\sqrt{2\pi\alpha}} f(x+z) \tag{1.25}$$

which can be generalised into operators, one can rewrite 1.24 into a more explicit form

$$\mathcal{O}_{\text{resummed}} = \int [Da] \exp\left[-\frac{1}{2}\int_{\boldsymbol{uv}} a(\boldsymbol{u})\boldsymbol{\Gamma}_2^{-1}(\boldsymbol{u},\boldsymbol{v})a(\boldsymbol{v})\right]\mathcal{O}_{\text{LO}}[A_{\text{init}} + a] \tag{1.26}$$

This results basically in averaging the classical trajectories over a set of initial conditions, done by the integral over a. This approach is called Classical Statistical Approximation (CSA) ([16, 40, 41]). It can be used to calculate observables. The right initial conditions in order to restore LO and NLO are:

$$\langle A^\mu \rangle = A^\mu_{\text{LO}}, \quad \boldsymbol{\Gamma}_2(\boldsymbol{u},\boldsymbol{v}) = \int \frac{d^2\boldsymbol{k}}{(2\pi)^3 2\omega_{\boldsymbol{k}}} a_{\boldsymbol{k}}(\tau_0,\boldsymbol{u}) a^*_{\boldsymbol{k}}(\tau_0,\boldsymbol{v}), \quad \lim_{x^0\to-\infty} a_{\boldsymbol{k}}(x) = e^{ik\cdot x} \tag{1.27}$$

which reflects the vacuum early times as well the narrow Gaussian distribution around the lowest order fields. The mode functions have to obey a linearized Yang-Mills-equation, and need to be solved for this until the time when the simulation would start, for which solutions exist [42]. This approach

could be used to study the process of thermalization from CGC initial conditions. However, an alternative related strategy in kinetic theory is in general of lower computational cost and based on similar assumptions as the CSA. A short look on the underling Schwinger-Keldysh formalism at finite temperature will be taken, which is a more intuitive way of calculating the interesting observables and will shed more light on the process of thermalization.

Chapter 2

The Boltzmann equation

2.1 Kadanoff-Baym equations and Wigner transform

We have seen that for gluon saturation, one can describe a heavy ion collision with classical field theory and the right initial conditions. After the very early stages, the occupation number will decrease until being of order 1. This is due to the fact that after the very first stage, expansion happens and energy is transferred to the soft gluons, leading to thermalization in the end. From occupation numbers smaller than $\frac{1}{\alpha_s}$ on, the Boltzmann equation should be a correct description of the system [5, 15]. Therefore, there exists a range of the occupation number in which the description by the Boltzmann equation and by classical fields with the CGC framework are both valid, allowing a dual description. The kinetic approach can help develop intuitive pictures for understanding results from classical field simulations. An example is the occurrence of a Bose-Einstein-Condensate starting with overpopulated initial conditions, which was predicted first from the kinetic evolution [43], and was less obvious classical field description. It is extremely useful to have such dual descriptions as an important tool to develop deeper understanding and have mutual confirmation for interesting results from each other. Therefore, the aim is now to show how the Boltzmann equation arises from quantum field theory. This will be done in the simple framework of a scalar field theory with a ϕ^4 interaction term. It can be easily generalised to high energy QCD [44].

A possible starting point are the well known Dyson-Schwinger-equations in the Schwinger-Keldysh formalism

$$\begin{aligned} G(x,y) =& G^0(x,y) + \int_{\mathcal{C}} d^4u d^4v G^0(x,u)(-\Sigma(u,v))G(v,y) \\ G(x,y) =& G^0(x,y) + \int_{\mathcal{C}} d^4u d^4v G(x,u)(-\Sigma(u,v))G^0(v,y) \end{aligned} \tag{2.1}$$

These equations express how to resum the self energy in the propagators, with the free propagator G^0 and the resummed one, G. Both formulations are equivalent. One can now apply $(\Box + m^2)$ for both coordinates in order to obtain the following equations

$$\begin{aligned} (\Box_x + m^2)G(x,y) &= -i\delta_{\mathcal{C}}(x-y) + \int_{\mathcal{C}} d^4v \Sigma(x,v)G(v,y) \\ (\Box_y + m^2)G(x,y) &= -i\delta_{\mathcal{C}}(x-y) + \int_{\mathcal{C}} d^4v G(x,v)\Sigma(v,y) \end{aligned} \tag{2.2}$$

with $\delta_{\mathcal{C}}$ being the straightforward generalisation of the delta function to the time contour. These are the Kadanoff-Baym equations.

In order to reach the Boltzmann equation, one has do an approximate description, as kinetic theory is expressed by a particle distribution $f(x, \boldsymbol{p})$ which clearly violates the uncertainty principle. During the process, one will switch the description from quantum to classical many-body functions, which often involves the use of the Wigner-transform (for example [45]). This is related to the fact that for an off-equilibrium situation as this which is varying slowly in space and time, there is no invariance under translations. Instead, one uses a Fourier transform over the separation variable. This, together with the then existing dependency of the mid-point variable, will in the end allow to make use of the separation of degrees of freedom between hard and soft modes. The Wigner transform for an arbitrary 2-point function F is defined via

$$F(X,p) = \int d^4 s e^{ip\cdot s} F\left(X + \frac{s}{2}, X - \frac{s}{2}\right) \tag{2.3}$$

with the separation $s = x - y$ and the mid-point $X = (x+y)/2$, as well as the time integration over the real time axis and not the contour. The Kadanoff-Baym equations contain the convolution of the self-energy and the dressed propagator. It is therefore important to know how the Wigner transform behaves with respect to convolutions, which can be proven for a convolution of F and G to result in

$$H(X,p) = F(X,p) \exp\left\{\frac{i}{2}\left[\overleftarrow{\partial}_X \vec{\partial}_p - \vec{\partial}_X \overleftarrow{\partial}_p\right]\right\}) G(X,p). \tag{2.4}$$

The superscript arrows indicate the direction of action of the operator.
With the definition of the new variables, one easily sees that the derivatives in the Kadanoff-Baym equations can be rephrased in X and s. Due to this, the Wigner transform will in this case just be equal to a transformation $\partial_s \to -ip$.
We get then

$$\begin{aligned}
(\frac{1}{4}\Box_X - i\partial_X p - p^2 + m^2) G(X,p) &= -i + \Sigma(X,p) \exp\left\{\frac{i}{2}\left[\overleftarrow{\partial}_X \vec{\partial}_p - \vec{\partial}_X \overleftarrow{\partial}_p\right]\right\}) G(X,p) \\
(\frac{1}{4}\Box_X + i\partial_X p - p^2 + m^2) G(X,p) &= -i + G(X,p) \exp\left\{\frac{i}{2}\left[\overleftarrow{\partial}_X \vec{\partial}_p - \vec{\partial}_X \overleftarrow{\partial}_p\right]\right\}) \Sigma(X,p)
\end{aligned} \tag{2.5}$$

The Boltzmann equation is now a result of two approximations.

2.2 Approximations towards kinetic theory

Gradient approximation

The gradient approximation is based on the assumption that the derivatives with respect to X should be negligible with respect to the ones in s. The reason is that X is the scale of change of the properties of the system, e.g. the particle distribution, and by this much greater than the De Broglie wavelength of the particles, which is related to p. One can therefore say $p \sim \partial_s \gg \partial_X$. Due to this, the exponential in 2.5 can be neglected beyond the first term of its expansion. Taking the difference

of both equations and breaking the propagator and the self energy down into the $++$, $+-$, $--$ and $-+$ components gives after some calculations ([46, 47])

$$\begin{aligned} -2ip \cdot \partial_X (G_{+-}(X,p) - G_{-+}(X,p)) &= 0, \\ -2ip \cdot \partial_X (G_{+-}(X,p) + G_{-+}(X,p)) &= 2[G_{-+}\Sigma_{+-} - G_{+-}\Sigma_{-+}]. \end{aligned} \tag{2.6}$$

Quasi-particle approximation

Closely related to the Schwinger-Keldysh-formalism in thermal equilibrium, a local particle distribution $f(X, \boldsymbol{p})$ modifies the dressed propagators. This approximation is valid only for infinitely long-lived particles, but is still justified if the life-time of particles, that means, the time between two collisions is considerably larger then its wavelength. If one defines $\rho(X,p) = G_{-+}(X,p) - G_{+-}(X,p)$, the propagators become

$$\begin{aligned} G_{-+}(X,p) &= (1 + f(X,\boldsymbol{p}))\rho(X,p), \\ G_{+-}(X,p) &= f(X,\boldsymbol{p})\rho(X,p). \end{aligned} \tag{2.7}$$

The particle distribution was chosen in order to fall back to the equilibrium propagators (which can be seen by taking the difference). In contrast to usual finite temperature field theory, the particle distribution is not a thermal phase space distribution but space-time dependent.

These two approximations are crucial in order to apply kinetic theory. A similar approach to achieve this approximation can also be found in [15]. 2.6 and 2.7 can be combined, which gives together with the expression of the spacetime derivative and of the four-vector of $\boldsymbol{p}$

$$[\partial_t + \boldsymbol{v_p} \cdot \nabla_x] f(X,\boldsymbol{p}) = \frac{i}{\omega_{\boldsymbol{p}}} \left[(1 + f(X,\boldsymbol{p}))\Sigma_{+-} - f(X,\boldsymbol{p})\Sigma_{-+} \right]. \tag{2.8}$$

$\boldsymbol{v_p} = \boldsymbol{p}/2\omega_{\boldsymbol{p}}$ is the velocity vector for particles of momentum $\boldsymbol{p}$. The right hand side is called the collision term and denoted $\mathcal{C}_{\boldsymbol{p}}[f; X]$. It is, just as the whole equation, spatially local as it contains only objects evaluated at X. However, the collision term is non-local in momentum. The left hand side derivative is called the transport derivative, and constant for particles being only dependent on $\boldsymbol{x} - \boldsymbol{v_p}t$ which is of course the case for non-interacting particles. From now on, it is assumed that the distribution function is spatially homogeneous, which results in dropping the spatial derivative. As a result, the notation of the space-time dependency is omitted, even if the distribution is still time-dependent.

2.3 Calculation of the collision term

The description is for now restricted to a ϕ^4 point-like elastic interaction term of lowest order. In order to determine the Boltzmann equation explicitly, the self energies have to be computed, which is dependent of the underlying theory. They are usually truncated after the lowest non-zero order. In ϕ^4 theory, this is done at two-loops. The collision term is already known from the elastic scattering

cross section for a $2 \to 2$ process ([15, 17, 48]), as the amplitude becomes trivial here. It reads

$$\begin{aligned}\mathcal{C}_{\boldsymbol{p}}[f] = \frac{g^4}{4\omega_{\boldsymbol{p}}} \int_{\boldsymbol{p'kk'}} (2\pi)^4 \delta(P + K - P' - K')[f(\boldsymbol{p'}) f(\boldsymbol{k'})(1 + f(\boldsymbol{p})(1 + f(\boldsymbol{k})) \\ - f(\boldsymbol{p}) f(\boldsymbol{k})(1 + f(\boldsymbol{p'}))(1 + f(\boldsymbol{k'}))]\end{aligned} \tag{2.9}$$

with the conventional notation

$$\int_{\boldsymbol{k}} = \int \frac{d^3\boldsymbol{k}}{(2\pi)^3 2\omega_{\boldsymbol{k}}} \tag{2.10}$$

of the invariant phase space integral for on-shell-particles. $\boldsymbol{p}$ and $\boldsymbol{k}$ are initial, $\boldsymbol{p'}$ and $\boldsymbol{k'}$ are final particles. It describes the rate of change of the particle distribution, with production terms for $\boldsymbol{p}$ weighted by $1 + f(\boldsymbol{p})$, and destruction terms for particles of this momentum weighted by $f(\boldsymbol{p})$. In fact, this term can be also expressed in the retarded-advanced formalism, resulting in the possibility to do the same classical approximations as for the CSA in perturbation theory (which is derived from the reformulation in path integral formulation of quantum field theory), as demonstrated in [18]. This shows the equivalence of both approaches.

This is done with help of a simple transformation matrix [17, 49]

$$\Omega_{\alpha\epsilon} = \begin{pmatrix} 1 & -1 \\ 1/2 & 1/2 \end{pmatrix} \tag{2.11}$$

giving the new propagators (the retarded, advanced and symmetric ones)

$$\mathcal{G}^0_{\alpha\beta} = \begin{pmatrix} 0 & G^0_A = G^0_{++} - G^0_{-+} \\ G^0_R = G^0_{++} - G^0_{+-} & G^0_S = \frac{1}{2}(G^0_{++} + G^0_{--}) \end{pmatrix} \tag{2.12}$$

The sources will be attached to propagator endpoints labelled 1, which are the lowest time endpoints of a retarded or advanced propagator. With this, one can calculate the new propagators from the Schwinger-Keldysh propagators and get

$$\begin{aligned} G^0_R(p) = G^0_{21}(p) &= \frac{i}{(p^0 + i\epsilon)^2 - \boldsymbol{p}^2 - m^2}, \\ G^0_A(p) = G^0_{12}(p) &= \frac{i}{(p^0 - i\epsilon)^2 - \boldsymbol{p}^2 - m^2}, \\ G^0_S(p) = G^0_{22}(p) &= 2\pi(\frac{1}{2} + f(\boldsymbol{p}))\delta(p^2 - m^2). \end{aligned} \tag{2.13}$$

It follows easily that one has to transform the self-energies in a similar way. One therefore gets

$$\begin{aligned} \Sigma_{+-} &= -\Sigma_{11} + \frac{1}{2}\Sigma_{12} - \frac{1}{2}\Sigma_{21} \\ \Sigma_{-+} &= -\Sigma_{11} - \frac{1}{2}\Sigma_{12} + \frac{1}{2}\Sigma_{21} \end{aligned} \tag{2.14}$$

The collision term in this formulation reads

$$\mathcal{C}_{\boldsymbol{p}}[f] = \frac{i}{2\omega_{\boldsymbol{p}}} \left[\Sigma_{11}(P) + (f(\boldsymbol{p}) + \frac{1}{2})(\Sigma_{21}(P) - \Sigma_{12}(P))\right] \tag{2.15}$$

The self-energies are by definition imaginary, so that the collision term is real as required. For the vertices, one can use the rule

$$\Gamma_{\alpha\beta\gamma\delta} = -ig^2[\Omega^{-1}_{+\alpha}\Omega^{-1}_{+\beta}\Omega^{-1}_{+\gamma}\Omega^{-1}_{+\delta} - \Omega^{-1}_{-\alpha}\Omega^{-1}_{-\beta}\Omega^{-1}_{-\gamma}\Omega^{-1}_{-\delta}] \tag{2.16}$$

which results in

$$\Gamma_{1111} = \Gamma_{1122} = \Gamma_{2222} = 0, \quad \Gamma_{1222} = -ig^2, \quad \Gamma_{1112} = -ig^2/4. \tag{2.17}$$

This approach is identical for the CSA in pertubation theory. There, the CSA amounts to setting the vertex Γ_{1112} and of course also its permutations to zero [18], which is a result of the great strength of a source. Indeed, such a vertex would only have one source attached and would be less likely to occur. The identical approximation can be done also in the context of kinetic theory, so that an approximated collision term is derived, giving further insights about the influence of the ultraviolet cutoff [17]. However, in this work the focus lies on working with the full, unapproximated collision term 2.9.

2.4 Introducing Bose-Einstein condensate

$2 \to 2$ processes allow initial conditions which cause an excess of particles, as they can not be accommodated in the final Bose-Einstein distribution. For a dense gluonic system in perturbative QCD, this has already been observed [50]. The reason is the large occupation number of order g^{-2}, giving values for the particle density of $n \sim \frac{Q_S^3}{g^2}$ and for the energy density $\epsilon \sim \frac{Q_S^4}{g^2}$ and by this $n\epsilon^{-3/4} \sim g^{-1/2} \gg 1$. The system is overoccupied if $n\epsilon^{-3/4}$ is of order greater than one.

Any extra particles can form a Bose-Einstein condensate (BEC) at fixed $\boldsymbol{p} = 0$. If this is realised depends on the underlying theory and the strength of overoccupation. For the ϕ^4 model, number changing effects are small and therefore a condensate will arise. However, it will be transient, as the true equilibrium has no condensate, as it is expanding. In QCD, the inelastic processes are much stronger and will change the nature of the condensate. However, it was shown that these processes result in a speed-up of the condensation [51], but it will arise nevertheless. As for the here observed model only elastic interactions are considered, the conservation laws force the system to keep the number of particles constant. This can be accommodated in our formalism by modifying the particle distribution function as

$$f(\boldsymbol{p}) \to f(\boldsymbol{p}) + n_C(2\pi)^3\delta(\boldsymbol{p}) \tag{2.18}$$

It is implicitly assumed that for a small sphere of radius ϵ around zero, the integral over this sphere of the particle distribution $f(\boldsymbol{p})$ goes to zero for $\epsilon \to 0$. Applying this modification inside the Boltzmann equation and using it to simplify the integrals leads to coupled equations. Terms of higher than linear order in the condensate density cancel, as this includes two Dirac deltas, which simplifies the integrals down to the point that they either vanish due to kinematics or due to the fact that loss and gain terms cancel. The form of the arising coupled differential equations can be taken from [52] and reads

in this notation as:

$$\begin{aligned}\partial_t f(\boldsymbol{p}) = \frac{g^4}{4\omega_{\boldsymbol{p}}} \int_{\boldsymbol{p'kk'}} & (2\pi)^4 \delta(P + K - P' - K') \\ & \times [f(\boldsymbol{p'}) f(\boldsymbol{k'})(1 + f(\boldsymbol{p}))(1 + f(\boldsymbol{k})) \\ & - f(\boldsymbol{p}) f(\boldsymbol{k})(1 + f(\boldsymbol{p'}))(1 + f(\boldsymbol{k'}))] \\ + \frac{g^4 n_C}{8m\omega_{\boldsymbol{p}}} \int_{\boldsymbol{p'k'}} & (2\pi)^4 \delta(\omega_{\boldsymbol{p}} + m - \omega_{\boldsymbol{p'}} - \omega_{\boldsymbol{k'}}) \delta(\boldsymbol{p} - \boldsymbol{p'} - \boldsymbol{k'}) \\ & \times [f(\boldsymbol{p'}) f(\boldsymbol{k'})(1 + f(\boldsymbol{p})) \\ & - f(\boldsymbol{p})(1 + f(\boldsymbol{p'}))(1 + f(\boldsymbol{k'}))] \\ + \frac{g^4 n_C}{4m\omega_{\boldsymbol{p}}} \int_{\boldsymbol{kk'}} & (2\pi)^4 \delta(\omega_{\boldsymbol{p}} + \omega_{\boldsymbol{k}} - m - \omega_{\boldsymbol{k'}}) \delta(\boldsymbol{p} + \boldsymbol{k} - \boldsymbol{k'}) \\ & \times [f(\boldsymbol{k'})(1 + f(\boldsymbol{p}))(1 + f(\boldsymbol{k})) \\ & - f(\boldsymbol{p}) f(\boldsymbol{k})(1 + f(\boldsymbol{k'}))]\end{aligned} \tag{2.19}$$

as well as

$$\begin{aligned}\partial_t n_C = \frac{g^4 n_C}{4m} \int_{\boldsymbol{p'kk'}} & (2\pi)^4 \delta(m + \omega_{\boldsymbol{k}} - \omega_{\boldsymbol{p'}} - \omega_{\boldsymbol{k'}}) \delta(\boldsymbol{k} - \boldsymbol{p'} - \boldsymbol{k'}) \\ & \times [f(\boldsymbol{p'}) f(\boldsymbol{k'})(1 + f(\boldsymbol{k})) \\ & - f(\boldsymbol{k})(1 + f(\boldsymbol{p'}))(1 + f(\boldsymbol{k'}))].\end{aligned} \tag{2.20}$$

One may note that the condensate density will show an exponential behaviour. However, when this will induce also a time-dependent change of the functional of the distribution functions, a very fast change of the condensate density will be observed. Using the symmetry and antisymmetry of these equations, one can determine the following conservation laws:

$$\begin{aligned} n_C + \int \frac{d^3\boldsymbol{p}}{(2\pi)^3} f(\boldsymbol{p}) &= \text{const} \\ m n_C + \int \frac{d^3\boldsymbol{p}}{(2\pi)^3} \omega_{\boldsymbol{p}} f(\boldsymbol{p}) &= \text{const} \\ \int \frac{d^3\boldsymbol{p}}{(2\pi)^3} \boldsymbol{p} f(\boldsymbol{p}) &= \text{const} \end{aligned} \tag{2.21}$$

It becomes obvious that the condensation process strongly changes the development of the equilibrium, due to its influence on the two terms of 2.19. Without the condensate (e.g. in underoccupied systems), the final thermalization process is not triggered by the evolvement of the condensate but starts immediately, causing a higher influence of the initial conditions. Also, the high occupation significantly decreases the mean free path and amplifies the scattering, to an order of $\frac{1}{g^4} g^2 g^2 \sim 1$. This is a result of the Bose enhancement term $(1 + f(\boldsymbol{p}))$ which scales like 1 in the dilute and like $f(\boldsymbol{p})$ in the dense regime. Even if the coupling is small, it behaves like strongly interacting matter.

Starting from initial conditions, one can now solve 2.19 and 2.20 numerically. Due to the H-theorem [17, 53], the fixed point at infinite time for given initial conditions for the Boltzmann equation is known as being Bose-Einstein distributions with chemical potential in our case of particle number conservation, and are always reached. As the Boltzmann approach is strongly connected with the CSA, as has been demonstrated, this will give insight about the thermalization process at the early

stages of heavy ion collisions. On the other hand, it can be solved with a simple Euler method, a great advantage in comparison to conventional CSA. The conservation laws in 2.21 play also a central role here - they can be used to determine the quality of the numerical solution. This will be explained in more detail in the next chapter.

Chapter 3

Numerical setup

The Boltzmann equation has multiple advantages compared to the CSA. The higher flexibility in the choice of the classical approximations as done in [17] and the "exact" result as the reference on the one hand, but also the reduced numerical cost and the more intuitive interpretation on the other hand. In the CSA, the same calculation has to be repeated several times with smaller and smaller lattice spacing [16], which is not needed here. Instead, one can construct now an efficient deterministic Boltzmann solver. However, several steps need to be done in order to reach a fast and accurate simulation. These will be presented here, based on the algorithm used in [17].

3.1 Choice of constants

The first assumption made is that the distributions are isotropic, which allows to drop the $\boldsymbol{p}$ dependency in the distribution function in favour of a dependency of the modulus, which is a considerable simplification. The initial distribution which will be most commonly used in the following is such that the distribution is high below a characteristic momentum scale Q and vanishing above, as it is approximately the case for the initial Glasma. For the Glasma in heavy ion collisions, the phase space is maximally filled: $f_0 \sim 1/\alpha_S$. The simplest form of this is a scaled, shifted and mirrored Heaviside-distribution. It will be referred to as the CGC-like initial distribution. In order to avoid Q becoming an additional parameter of the problem, all dimensionful quantities will be expressed in units of Q. In the present case, Q is set to 1. It shall be noted that Q is the saturation scale discussed earlier.

It is possible to make the same choice for the coupling constant g. Indeed, as it is only present as fourth power in front of the collision term, it only controls the speed of the reactions. From 2.20 it is obvious that a condensate can only exist if there were particles in it already at the initial state. The existence of a condensate is necessary as for overoccupied initial conditions, instabilities would occur at the time when transition into the condensate would otherwise happen. To prevent this, a negligible initial value of n_C is used as initial condition, at a value of 10^{-5}. The exact value has no visible effect on the simulation (see [17]).

Both 2.19 and 2.20 are mass dependent. The behaviour of this equations for masses going to zero requires more investigation. The mass is therefore chosen to be small but non-zero, with the constant value $m = 0.1Q$. This is indeed a possibility for further improvements. As the simulation is intended to investigate gluons, one could also include their dynamical mass instead fixing the mass. Indeed, gluons show the behaviour of having an effective mass arising from their interactions, making it momentum dependent ([54, 55]).

The self energies of gluons do not vanish on the mass shell in vacuum due to the interactions of gluons with the surrounding bath, which changes the dispersion relation. This results in massive bosons even if they are massless without interactions (i.e. $g = 0$). There are two different poles of the gluon-propagators, a longitudinal and a transverse one, with the longitudinal one being purely collective which decouples for momenta much higher than the temperature [47]. One could include this behaviour by calculating the running mass at each point in the simulation, using one of the possible approximations of the dispersion relation of the mass investigated [56]. However, having a non-fixed mass will result in a violation of the energy conservation. Instead, one could use a fixed mass which is not set by hand but instead calculated with the use of the final distribution which is known from the initial parameters. Such a possible improvement is out of the scope of this report.
With this choice of parameters, one can start defining the grid and the integration strategy.

3.2 Discretization and timestep

The time integration itself will be done with the Euler method, as it has low computational cost and is in most cases of sufficiently high accuracy. However, it can become unstable in the vicinity of the transition towards the condensate. There is a lot of freedom in the choice of how to modify the timestep. One possibility is the following:
Starting with a timestep of 1, it is

- reduced if the relative or absolute change in the number of particles in the condensates lies over a threshold
- reduced if at one of the gridpoints the particle distribution becomes negative, and the calculation for this step is repeated
- gradually increased up to a maximum of 1 if none of these occurs.

With this adaptive timestep, a stable simulation can be ensured. A parallel monitoring of conserved quantities ensures that the conservation laws are respected with machine accuracy. This is simplified by not including one feature of heavy ion collisions: the rapid expansion of the system in longitudinal direction. This changes the conservation laws dynamically and will be not included in this set-up. Instead, the thermalization is supposed to happen "in a box".

However, the right choice of the momentum discretization is crucial. The integrals over the momentum space have to be transformed into discrete sums. The problem lies in the energy conservation. Of the four momenta p, p', k, k', one is calculated when given the other three by energy conservation. However, this is not guaranteed to lie on a grid point, which would force one to inter-

polate, resulting in additional computational cost and errors. Instead, one may set up a linear grid in the energy, starting at m up until a UV-cutoff ω_Λ by $\omega_i = m + i\Delta$ with $\Delta \equiv \frac{\omega_\Lambda - m}{N}$ where N is the number of grid points. This then translates into a UV-cutoff for the momentum too. It will be in the following chosen to be $\frac{\Lambda_{UV}}{Q} = 4$. The quadrature formula becomes by this

$$\int_m^\Lambda d\omega f(\omega) \to \Delta \sum_{i=1}^{N} w_i f(\omega_i) \tag{3.1}$$

The zero gridpoint is excluded due to possible singularities. In fact, its contribution can be calculated separately using 2.19 and 2.20. w_i is the respective weight. The trapezoidal rule will be used, for which the weights are 1/2 at the first and last grid point, and 1 for all others.

In order to respect the conservation laws, the discretization has also to preserve the antisymmetry between initial and final states, as well as the symmetry between same state particles. It will shortly shown that there will be only two-dimensional integrals. In such, this is achieved by adding a third integral with a delta function of energy conservation

$$\int d\omega_{\boldsymbol{p}'} d\omega_{\boldsymbol{k}'} \cdots = \int d\omega_{\boldsymbol{p}'} d\omega_{\boldsymbol{k}'} d\omega_{\boldsymbol{k}} \delta(\omega_{\boldsymbol{p}} + \omega_{\boldsymbol{k}} - \omega_{\boldsymbol{p}'} - \omega_{\boldsymbol{k}'}) \dots \tag{3.2}$$

so that, in the present nomenclature, these laws hold. Due to discretization, when i is the fix index of $\omega_{\boldsymbol{p}}$, this leads to the following weights

$$\Delta^2 \sum_{j,k,l=1}^{N} w_j w_k w_l \delta_{i+j-k-l} \cdots = \Delta^2 \sum_{k,l=1}^{N} w_j w_k w_{k+l-i} \dots \tag{3.3}$$

3.3 Numerical evaluation of the collision term

For spatially homogeneous systems, the condensation transition should be a genuine discontinuity. However, this is not exact after discretization, as there is always a momentum greater than zero which is the smallest and defines the maximal size of the system. However, the reproduction of the discontinuity improves with the resolution of the grid. This means that one would like to have a high value for N, the number of energy grid points. This is however limited by the computation time. Indeed, integrals are very costly. Looking at 2.9, one sees an integral over three 3-dimensional phase-spaces and 4 constrains on energy and momentum, giving a 5-dimensional integral. This integral is unaffected by the introduction of the condensate and still present in 2.19. As this would have to be evaluated for each $\boldsymbol{p}$ at every timestep, the computational cost would scale as N^6 times the number of steps. Under this conditions, no satisfying resolution could be achieved. Gladly, it is possible to reduce the integral to two dimensions, just as the other integrals in 2.19. In a first step, the strategy of [17] is reviewed. In a second step, a generalisation is presented which allows an application on a greater number of cases.

3.3.1 Direction independent scattering

When the assumption is made that the distribution is isotropic in space and the direction of the particles in the scattering process does not influence the coupling like for the ϕ^4 interaction, the

angular integrations can be completely separated. The approach has been demonstrated in Appendix A of [57] and Appendix B of [17] but will be outlined here as a reminder. For a momentum $\boldsymbol{p}$, the angular measure reads $d\Omega_{\boldsymbol{p}} = \sin\theta_{\boldsymbol{p}} d\theta_{\boldsymbol{p}} d\phi_{\boldsymbol{p}}$ and one knows that $\int d\Omega_{\boldsymbol{p}} = 4\pi$ with $\phi_{\boldsymbol{p}}$ being the azimuthal and $\theta_{\boldsymbol{p}}$ the polar angle. As the angular dependency can be separated due to our assumption, it holds that

$$\mathcal{C}_{\boldsymbol{p}}[f] = \frac{1}{4\pi} \int d\Omega_{\boldsymbol{p}} \mathcal{C}_{\boldsymbol{p}}[f] \tag{3.4}$$

Now, one may also use the well known identity

$$\delta(\boldsymbol{p} + \boldsymbol{k} - \boldsymbol{p}' - \boldsymbol{k}') = \frac{1}{(2\pi)^3} \int d^3\boldsymbol{x} e^{i(\boldsymbol{p}+\boldsymbol{k}-\boldsymbol{p}'-\boldsymbol{k}')\cdot\boldsymbol{x}} \tag{3.5}$$

Applying it to the collision term in which the angular integrations had been separated out, as well as expanding the used notation for the momentum integral lets a term appear of the form

$$\frac{p'kk'}{64\pi^5 \omega_{\boldsymbol{p}}\omega_{\boldsymbol{k}}\omega_{\boldsymbol{p}'}\omega_{\boldsymbol{k}'}} \int x^2 dx \int e^{i\boldsymbol{p}\cdot\boldsymbol{x}} d\Omega_{\boldsymbol{x}} \int e^{i\boldsymbol{p}'\cdot\boldsymbol{x}} d\Omega_{\boldsymbol{p}'} \int e^{i\boldsymbol{k}\cdot\boldsymbol{x}} d\Omega_{\boldsymbol{k}} \int e^{i\boldsymbol{k}\cdot\boldsymbol{x}} d\Omega_{\boldsymbol{k}'} \tag{3.6}$$

This well-known integral can be solved, as the distribution functions are independent of the angles, giving

$$\frac{4}{\pi p \omega_{\boldsymbol{p}}\omega_{\boldsymbol{k}}\omega_{\boldsymbol{p}'}\omega_{\boldsymbol{k}'}} \int_0^\infty \frac{dx}{x^2} \sin(px)\sin(kx)\sin(p'x)\sin(k'x) \tag{3.7}$$

which results into [57]

$$\frac{1}{p\omega_{\boldsymbol{p}}\omega_{\boldsymbol{k}}\omega_{\boldsymbol{p}'}\omega_{\boldsymbol{k}'}} \mathrm{Min}(pkp'k'). \tag{3.8}$$

Using now the identity $pdp = \omega d\omega$ to achieve an integration over the energies and eliminating the remaining linear dependencies of the three not-fixed momenta and their energies in the denominator as well as using the delta function of the energy conservation to eliminate another integral leaves one with the two dimensional integration for the collision term of

$$\mathcal{C}_{\boldsymbol{p}}[f] = \frac{g^4}{128\pi^3 p\omega_{\boldsymbol{p}}} \int d\omega_{\boldsymbol{p}'} d\omega_{\boldsymbol{k}'} \mathrm{Min}(pkp'k') F[f] \tag{3.9}$$

where $F[f]$ is the dependency on the particle distribution for the chosen approximation. In practice, the integration domain is divided in four areas depending on the value of the minimum. This very elegant reduction of the dimensions of the integral can be calculated very fast and reaches high numerical resolutions. However, it comes with a high cost: as the angles are omitted, it is not possible to have the amplitude of the scatterings dependent on the value of the Mandelstam variables, which are angular dependent. Therefore, it is not possible to investigate theories with momentum dependent amplitudes with an algorithm based on this assumption. Indeed, all which was presented so far would have been equally possible for elastic $2 \to 2$ processes in other theories. Only an amplitude squared dependent of the Mandelstam variables, $G(s,t,u) = G(P,K,P',K')$ would have to be included in the terms. For this, the kinetic variables have to be restored, which is not possible with this reduction. In the following section, another, not yet considered reduction shall be presented, which fixes this constraint.

3.3.2 Generalisation

The crucial step in the last approach was separating the angular integrals in order to make use of the reformulation of the delta function and producing the separate sinus factors. Instead, one may perform a change of the integration variables by introducing a new momentum $\tilde{\boldsymbol{p}} = \boldsymbol{p} + \boldsymbol{k}$. The additional integral over this variable is compensed by another delta function, leading to a reformulated integral of the form

$$\frac{g^4}{4\omega_{\boldsymbol{p}}} \int_{\boldsymbol{p'kk'}} \int d^3\tilde{\boldsymbol{p}} (2\pi)^4 \delta(\omega_{\boldsymbol{p}} + \omega_{\boldsymbol{k}} - \omega_{\boldsymbol{p'}} - \omega_{\boldsymbol{k'}}) \delta(\tilde{\boldsymbol{p}} - \boldsymbol{p} - \boldsymbol{k}) \delta(\tilde{\boldsymbol{p}} - \boldsymbol{p'} - \boldsymbol{k'}) G(P, K, P', K') F[f]. \quad (3.10)$$

After expanding the notation of the integral as well as introducing an angular measure integration over $\frac{d\Omega_{\boldsymbol{p}}}{4\pi}$ (which is possible due to isotropy), applying again the relation $pdp = \omega d\omega$, multiplying by $1 = \frac{p}{p}$ and eliminating one integral with the energy delta function, one gets

$$\begin{aligned} \frac{g^4}{32\omega_{\boldsymbol{p}} p (2\pi)^5} \int & [d\tilde{p} d\omega_{\boldsymbol{p'}} d\omega_{\boldsymbol{k'}}] [d\Omega_{\boldsymbol{p}} d\Omega_{\boldsymbol{k}} d\Omega_{\boldsymbol{p'}} d\Omega_{\boldsymbol{k'}}] \\ & (\tilde{p}pk)(\tilde{p}p'k') \delta(\tilde{\boldsymbol{p}} - \boldsymbol{p} - \boldsymbol{k}) \delta(\tilde{\boldsymbol{p}} - \boldsymbol{p'} - \boldsymbol{k'}) G(P, K, P', K') F[f] \end{aligned} \quad (3.11)$$

with the scaling of the coupling $G(P, K, P', K')$ which will be the squared amplitude later on. At this point, one can show the equality to the old approach when setting $G \equiv 1$. In this case, it should be possible to restore the old result, as the delta functions are again independent of the polar and azimuthal angles of $\boldsymbol{p}$ and by this the whole integrand. One can take a look at this part of 3.11:

$$\begin{aligned} & \int d\Omega_{\tilde{\boldsymbol{p}}} d\Omega_{\boldsymbol{k}} \frac{d\Omega_{\boldsymbol{p}}}{4\pi} (\tilde{p}pk) \delta(\tilde{\boldsymbol{p}} - \boldsymbol{p} - \boldsymbol{k}) \\ &= \int_0^\infty \frac{dx}{x} 8 (\sin(\boldsymbol{x} \cdot \tilde{\boldsymbol{p}}) \sin(\boldsymbol{x} \cdot \boldsymbol{p}) \sin(\boldsymbol{x} \cdot \boldsymbol{k})) \\ &= \int_0^\infty \frac{dx}{x} 2 (-\sin(\boldsymbol{x} \cdot (\tilde{\boldsymbol{p}} - \boldsymbol{p} - \boldsymbol{k})) + \sin(\boldsymbol{x} \cdot (\tilde{\boldsymbol{p}} + \boldsymbol{p} - \boldsymbol{k})) \\ & \qquad + \sin(\boldsymbol{x} \cdot (\tilde{\boldsymbol{p}} - \boldsymbol{p} + \boldsymbol{k})) - \sin(\boldsymbol{x} \cdot (\tilde{\boldsymbol{p}} + \boldsymbol{p} + \boldsymbol{k})) \\ &= \pi \quad (\operatorname{sgn}(\boldsymbol{x} \cdot (\tilde{\boldsymbol{p}} + \boldsymbol{p} - \boldsymbol{k})) - \operatorname{sgn}(\boldsymbol{x} \cdot (\tilde{\boldsymbol{p}} - \boldsymbol{p} - \boldsymbol{k})) \\ & \qquad + \operatorname{sgn}(\boldsymbol{x} \cdot (\tilde{\boldsymbol{p}} - \boldsymbol{p} + \boldsymbol{k})) - \operatorname{sgn}(\boldsymbol{x} \cdot (\tilde{\boldsymbol{p}} + \boldsymbol{p} + \boldsymbol{k})) \end{aligned} \quad (3.12)$$

In the second line, the reformulation of the delta function was used and all the angular integrations could be executed, as the integral is now independent of the angles. The resulting integral is known and gives for our choice of variables, 2π. The same can be done for the second $\tilde{p}$ factor with the second delta function, by introducing the angular measure integration over p a second time, balanced again by a factor of $(4\pi)^{-1}$.

One is left with the following reformulation of 3.11 for $G \equiv 1$

$$\frac{g^4}{32\omega_{\boldsymbol{p}} p (2\pi)^3} \int d\tilde{p} d\omega_{\boldsymbol{p'}} d\omega_{\boldsymbol{k'}} F[f] \quad (3.13)$$

The length of the integration interval over $\tilde{p}$ has therefore to be equal to $2\,\mathrm{Min}(pkp'k')$ in order to restore the previous result of the old reduction in 3.9. This has to be the range of $\tilde{p}$, as the integration over $\tilde{p}$ is done over a trivial integrand. It is known that by construction, this interval ranges from

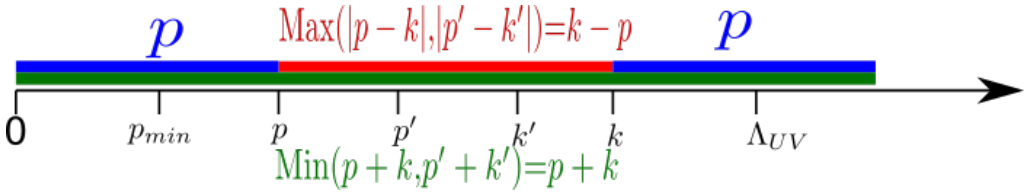

Figure 3.1 – Sketch of the range of the momentum moduli

$\mathrm{Max}(|p-k|,|p'-k'|)$ to $\mathrm{Min}(p+k,p'+k')$. Indeed, both formulations, $\tilde{\boldsymbol{p}}=\boldsymbol{p}+\boldsymbol{k}$ and $\tilde{\boldsymbol{p}}=\boldsymbol{p'}+\boldsymbol{k'}$ result in two restrictions each on the range of $\tilde{p}$. If both times the first or both times the second term in the maximum/minimum is chosen, this gives, depending on the sign inside the modulus, two times one of the four momenta as the length of the integration interval. This one being the minimum momentum of the four is a result of energy conservation. An example of such a case is shown in Figure 3.1. In this case, one of the pairs of momenta lies in between the other pair, which results in the described condition that the maximum/minimum always chooses the same pair. Then, as shown in the figure, is the interval length two times the minimum momentum. However, it is not clear that the case of figure 3.1 is always valid, in other words, that the range of the final momenta is always contained in the range of the initial momenta, or reversed. This shall be shown here.

Let p the minimum (all other cases follow by renaming the momenta). Then, due to relation between energy and momentum, $\omega_{\boldsymbol{p}}$ is the smallest of the four energies. As all energies are strictly positive, $\omega_{\boldsymbol{k}}$ has to be the greatest energy, resulting in k being the greatest momentum and by this, $|p-k|$ is greater than $|p'-k'|$. The square of the energy conservation equation is of the form

$$(p+k)^2-2pk+2\omega_{\boldsymbol{p}}\omega_{\boldsymbol{k}}=(p'+k')^2-2p'k'+2\omega_{\boldsymbol{p'}}\omega_{\boldsymbol{k'}} \tag{3.14}$$

The result follows if $\omega_{\boldsymbol{p}}\omega_{\boldsymbol{k}}-pk$ is greater for $|p-k|$ being greater. For this, one can take a general view on the equivalent function $f(x,y)=\sqrt{x^2+m^2}\sqrt{y^2+m^2}-xy$. The partial derivative with respect to x is $\partial_x f(x,y)=x\frac{\sqrt{y^2+m^2}}{\sqrt{x^2+m^2}}-y$ which becomes zero only for $x\equiv y$. An evaluation of the signs left and right of the zero point shows that this is an minimum. The same analysis can be done in y-direction. This observation can be also made clearer with help of figure 3.2. One can see that the value of $f(x,y)\widehat{=}\omega_{\boldsymbol{p}}\omega_{\boldsymbol{k}}-pk$ is increasing with increasing difference between x and y, which was needed for the proof. The minimum is found at points where $x\equiv y$ is true, e.g. for two equal momenta. By this, this term is greater for momentum pairs with a higher difference, which was the desired statement.
In summary from p being the minimum, it follows that $|p-k|$ is greater than $|p'-k'|$, and also that $p+k$ is smaller than $p'+k'$. Due to this, the interval will evaluate to have a length of $2p$.

For the more interesting case of G being not constant, most of the integrals are trivial. As p (fixed as this is the momentum for which the derivative is performed) and k (due to the delta functions) are known, in the integral over $\tilde{p}$ the angles in the triangle between these three momenta are fixed. On top of that, $\tilde{\boldsymbol{p}}=\boldsymbol{p'}+\boldsymbol{k'}$ is equally true. When the integration is performed over the energy/momentum grid, these two momenta are also fixed, resulting in fixing the angle between them. The only angle which is then not fixed is the azimuth between the $\tilde{p}pk$ and the $\tilde{p}p'k'$ plane, over which there has

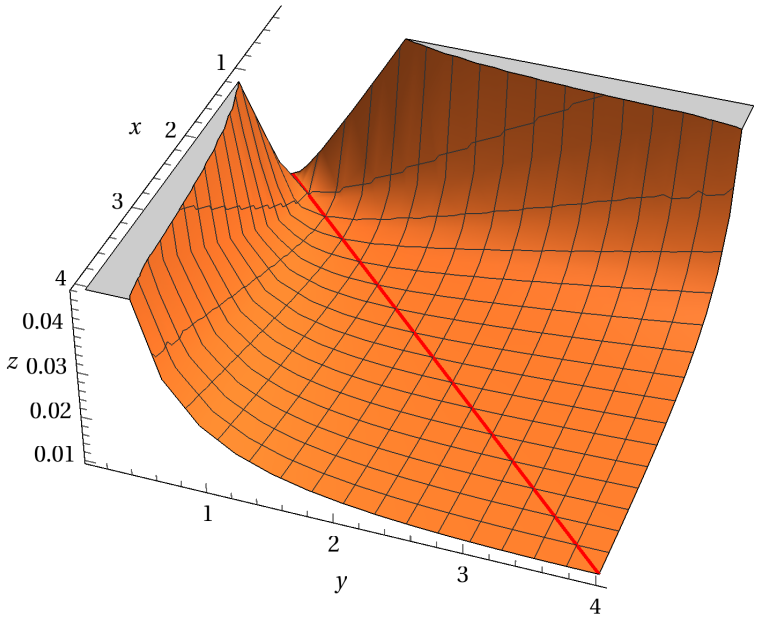

Figure 3.2 – $f(x,y) = \sqrt{x^2+m^2}\sqrt{y^2+m^2} - xy$ in a typical momentum range. The curve on which $\partial_x f(x,y) \equiv \partial_x f(x,y) \equiv 0$ is marked in red.

to be done the fourth integration, together with the still present $d\omega_{\boldsymbol{p}'}$ and $d\omega_{\boldsymbol{k}'}$ as well as the new $\tilde{p}$ integration. With this knowledge, it is possible to reuse the old integration algorithm. The change is merely replacing the minimum function with an integration over the $\tilde{p}$ interval, by using again the trapezoidal rule, as well as dropping a 2π factor and instead integrating over this angle. At each of this integration steps, the Mandelstam variables can now be calculated, with which G can be evaluated, which is used to scale the the contributions to the integral which had been present before.

3.4 Calculation of Mandelstam variables

Indeed, the calculation of the Mandelstam variables is at this point easily possible. $\tilde{P}$ (the 4-vector to $\tilde{p}$) itself is the corresponding vector to s, so $s = \tilde{P}^2$. u can be calculated by $4m^2 - s - t$. One is left with determining t.

$$t = (P - P')^2 = 2m^2 - 2\omega_{\boldsymbol{p}}\omega_{\boldsymbol{p}'} + 2\boldsymbol{p}\boldsymbol{p}'. \tag{3.15}$$

The last term becomes in cartesian coordinates

$$2[(p\cos(\alpha))(p'\cos(\beta)) + (p\sin(\alpha))(p'\sin(\beta))\cos(\Psi)] \tag{3.16}$$

with α, β being the angles in the $\tilde{p}pk$ and the $\tilde{p}p'k'$ plane between $\tilde{p}$ and the respective momentum, and Ψ the azimuthal angle over which the integration is done, e.g. the azimuthal angle of one of both planes if the zero point of the angle is set in the other plane. The sines can be determined knowing that the area of a triangle with edges a, b and c is given by $\frac{1}{2}ab\sin(\gamma)$ for γ the angle between a and b, and at the same time the area is given by Heron's formula as $\frac{1}{4}\sqrt{(a+b+c)(b+c-a)(a-b-c)(a+b-c)}$. This allows one to extract the sine. The cosine terms could be computed by trigonometric functions, or, numerically cheaper, by using $k'^2 = (\tilde{\boldsymbol{p}} - \boldsymbol{p}')^2$ and the equivalent formula for $\cos\alpha$. The resulting

relationships have only to be carefully formulated in order to avoid division by small numbers and achieve a high computation speed.

For each gridpoint of the energy grid (with N points), a grid in the momentum range of $\tilde{p}$ (with N_P points) is initialised, over which is integrated by the trapezoidal rule. The evaluation is done in the midpoint to avoid division by zero. For Ψ, a fourth of the integration interval needs to be covered. Indeed, one half can be neglected by the symmetry of the cosine. The second simplification can be achieved knowing that $p' \sin(\beta) = -k' \sin(\gamma)$. Therefore, integrating only from 0 to $\pi/2$ and taking the result times 4 is not equal to integrating over the full interval, but equals instead half the contribution for fixed p' and k' and half the contribution for exchanged roles. Therefore, due to summing over p' and k', one gets in the end the right result. This is indeed a huge improvement, which can theoretically reduce the computation speed by a factor four. The number of angle gridpoints was chosen in the following to be equal to N_P.

Nevertheless, this generalisation comes at a high computational cost. Even if the number integration points for Ψ and $\tilde{p}$ can be chosen smaller than N, these additional integrations have to be done for each gridpoint (p', k') at each timestep. Especially the setting up of the $\tilde{P}$ grid is a relevant slowdown. It would be desirable to do this once during the initialisation process and access it when needed. However, for a fixed number of integration points in the $\tilde{p}$ interval, the position of the grid points is different for each combination of p' and k' (up to switching) and would have to be saved for each of them, resulting for $N = 1024$ momentum values and $N_P = 12$ $\tilde{p}$ gridpoints in a memory need of over 80 GB, far more than was available for the upcoming simulations. Also, the reduced computation time would be compensed by the time needed to load the gridpoints. An alternative strategy was considered, by using a fixed step size instead of a fixed number of steps, which allows to reduce the amount of needed precalculated data by a factor of N. This solves the memory problem, however, a very small step size in $\tilde{p}$ is needed to not loose information about small-s-processes and a general trapezoidal integration formula needs to be used for the now unequally distributed integration points, resulting in highly increased computation time. Therefore, the grid over $\tilde{p}$ was dynamically computed when needed.

Chapter 4

Applications

In the following, the potential of this new algorithm for a deterministic Boltzmann solver with full angular dependence shall be demonstrated. Three examples of possible modifications of the coupling will be shown: cutoffs in the coupling as well as the more relevant amplitude of the gluon-gluon scattering and the ϕ^3 theory.

It shall be again mentioned that this new range of applications comes at a cost. The algorithm has to do a considerably higher number of computations. As the old algorithm could only compute the ϕ^4 theory, a comparison of performance is only possible in this case. The following table gives an idea of the slowdown due to the new algorithm.

	original algorithm	new algorithm
Average time per step	9.3s	17.1s

Table 4.1 – Comparison of the new and old algorithm in terms for a simulation with ϕ^4 interaction for N=1024 for both algorithms and N_P=12 for the new algorithm. Execution in two threads.

An average slowdown of 84% is observed. For more complex scattering amplitudes, the difference in computation time will increase. Due to this, the following simulations were done on a cluster with 16 cores, allowing a high parallelization. This is indeed a great advantage of the presented algorithm, which allows independent calculations of energy gridpoints and by this ensures a maximal efficiency of parallelization. This is crucial in order to reach reasonable computation times.

4.1 ϕ^4 theory with suppressed interactions for small or large momentum

The first application is motivated by the wish to verify the legitimacy of the approach. Choosing a very high upper cutoff value should in fact have no change on the outcome at all. However, the function of the cutoff has to be carefully chosen. If it does not respect the symmetries of the system, the conservation laws might be violated. The integrand is symmetric under the exchanges $P \leftrightarrow K$ and $P' \leftrightarrow K'$ as well antisymmetric as under $(P, K) \leftrightarrow (P', K')$. A possible choice is therefore

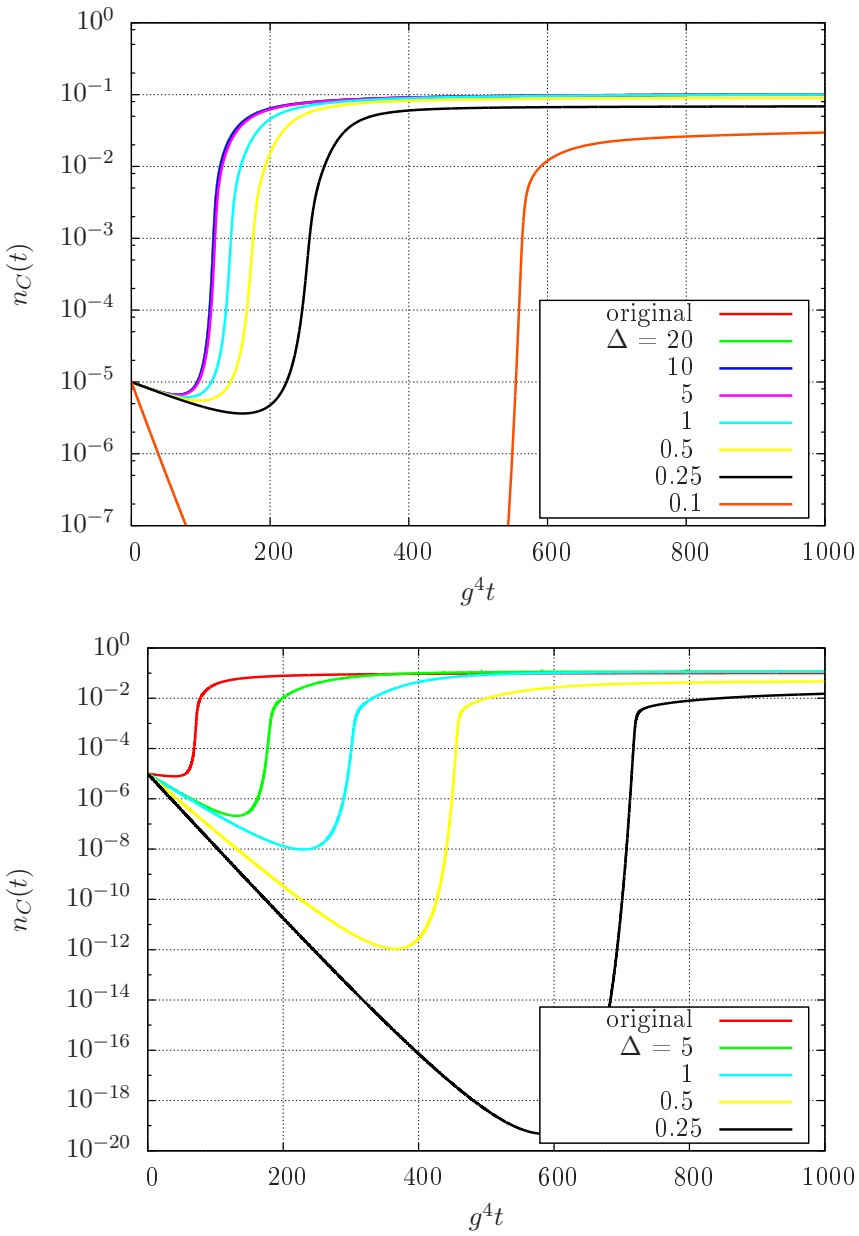

Figure 4.1 – Development of the particle density in the condensate in a simulation with N=1024. Original code from [17] in comparison with modified code for different values of a upper cutoff Δ. Top: CGC-like initial conditions. Bottom: exponential initial distribution.

to compare the cutoff with the value of $G(s,t,u) = s^2 + t^2 + u^2$, which naturally respects these symmetries. This will be done with the Heaviside-distribution, via

$$\theta(\Delta - G(s,t,u)) \tag{4.1}$$

Figure 4.1 shows at the top the time evolution of the density of condensed particles for the CGC-like initial condition

$$f(0,p) = f_0\theta(Q-p) \tag{4.2}$$

for a coupling of the form 4.1, as well as the result with the same initial conditions of the code of [17] for momentum independent interactions. In a first observation, one can see that the graph of

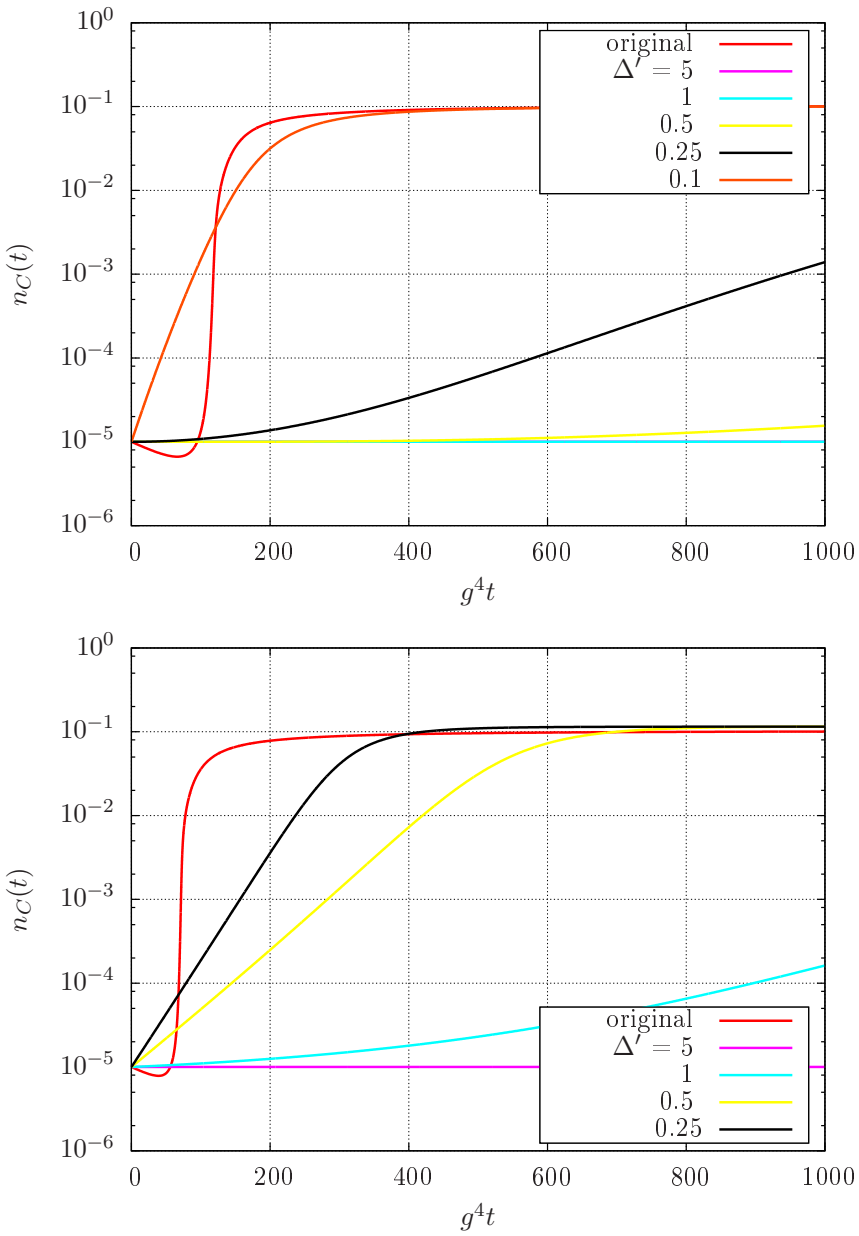

Figure 4.2 – Evolution of the particle density in the condensate in a simulation with N=1024. Original code from [17] in comparison with modified code for different values of a lower cutoff Δ'. Top: CGC-like initial conditions. Bottom: exponential initial distribution.

the unmodified code is visually identical to the graphs for a cutoff of 20 and 10. This does not only support the claim that the generalisation is consistent with the old results, as it restores the original outcome for high cutoffs. It also sheds light on the process of condensation. As for this run, the maximum allowed momentum was of value 4, the high Δ were in fact reached. Processes of particles of high energy exchanging energy with low energy particles were suppressed, but this resulted in almost no visible effects. With the given CGC initial conditions, the infrared contributions control the initial slope, which is almost identical for all cases except $\Delta = 0.1$. This is due to the fact that for the choice of the initial maximum momentum of $Q = 1$, the maximum value for $s^2 + t^2 + u^2$ is of the order of m^2 and lies by this lower for all cutoffs greater than 0.1.

This can be made plausible by a short calculation. For the case that the particle corresponding to p lies in the condensate and for small masses, one has

$$s^2 + t^2 + u^2 = 4m^2(\omega_{\boldsymbol{k}}^2 + \omega_{\boldsymbol{p}'}^2 + \omega_{\boldsymbol{k}'}^2) + \mathcal{O}(m^3). \tag{4.3}$$

Now, for the cutoff to influence the calculation one needs

$$\frac{\Delta}{4m^2} \leq \omega_{\boldsymbol{k}}^2 + \omega_{\boldsymbol{p}'}^2 + \omega_{\boldsymbol{k}'}^2. \tag{4.4}$$

But for Δ=0.25 and m=0.1 this gives 6.25, a value which cannot be reached by the right hand side for the initial condition. For $\Delta = 0.1$, the left hand side gives 2.5. This can be also not reached for all momenta corresponding to the energies smaller than $Q = 1$. However, 2.20 allows processes with zero momentum distributions involved, as long as they preserve energy conservation, which is for the chosen mass just enough let processes arise which are suppressed for this value of the cutoff under this initial conditions. Nevertheless, the energy conservation prevents that unoccupied channels of such high energy are accessed that a cutoff of 0.25 has influence on the initial slope, as a sum of energies over 6 cannot be achieved with either the ingoing momentum being smaller than 1 or both outgoing. This explains why the slope only changes for $\Delta = 0.1$ in figure 4.1, as for only such a cutoff, the interaction was modified.

If an initial condition is chosen where hard particles exist, the slope will not be constant for all cutoffs, as the cutoff-value is always reached due to the hard particles. This becomes visible in the lower figure of 4.1, where for comparison the evolution starting with a Bose-Einstein initial distribution of the form

$$f(p) = \frac{10}{\exp\left(\sqrt{p^2 + 0.25} - 1\right)} \tag{4.5}$$

is shown. Note that this is not the equilibrium distribution for this system as otherwise no time evolution would be observable.

For cutoffs which enter the infrared zone, less momentum is transferred, which slows down the condensation process and gives more time to the condensate to lose particles. This explains the shift of the transition point in both figures. If the cutoff reaches the order of m^2, the simulation becomes unstable, as almost all interactions get suppressed. Although it seems that for stricter cutoffs not the same maximum condensate density level is reached, due to the H-theorem, it is known that the same value will be reached for $t \to \infty$. The evolution towards the final condensate density has been slowed down by the cutoff. The difference in the equilibrium condensate density levels between the upper and lower figure of figure 4.1 can be explained by the different equilibrium condensate density due to the difference in the initial conditions.

In figure 4.2 all interactions below a certain value of $s^2 + t^2 + u^2$ are suppressed, realised by a cutoff function like

$$\theta(G(s, t, u) - \Delta'). \tag{4.6}$$

The condensation process is governed by the infrared regime. Only when the cutoff does not suppress this regime completely, the condensation can happen. However, at no point the condensate density

decreases, the transition starts immediately with a cutoff-dependent slope, which goes to zero for a complete cutoff of the infrared domain.

This strong dominance of the infrared regime here, which suppresses the loss of condensate particles, is not caused by the CGC-like initial condition like for the UV cutoff. This becomes evident as one can see the same behaviour for both the CGC-like initial condition as for the exponential initial condition. For the CGC-initial condition, for cutoffs stricter than Δ'=0.1, there are again initially no particles with a momentum greater than Q (as explained before). If there are only soft particles and a high cutoff, no interaction is possible which has high enough values for the energies as in the initial distribution the sum of the energies can not exceed the value of $\frac{\Delta'}{4m^2}$. The momentum distribution has to develop hard particles in order for the condensation to set in. This is again not the case for Δ'=0.1 and for the smaller cutoffs of the exponential initial distribution, for which the condensation sets in immediately. However, even if Δ' is set low enough so that this value is exceeded, one can see no loss of condensate.

This observation becomes more clear when one takes a look at distribution dependence of the condensate density development in 2.20. This dependence can be reformulated to read

$$f(p')f(k') - f(k) - f(k)f(p') - f(k)f(k') \tag{4.7}$$

The condensate density is increased by interactions with final particles having a product of their distributions being higher than distribution of the second initial particle added by the product of their distributions with this particle. The energy conservation restricts the possible combinations, and restricts the final momenta to be smaller than k. Just as the CGC initial distribution, the exponential one favours infrared particles too. As a consequence, this term is much smaller if one of the final momenta is close to k and the other one small, as the distribution function for the small momentum will be higher. Additionally, the main loss terms are from interactions with a low value for k due to the higher distribution in the infrared zone. This shows that the most important contributions to a loss of condensate density arise from interactions which are in the deep infrared region, which is suppressed by the cutoff. One therefore sees that interactions with a very low invariant mass and momentum transfer cause a loss in condensate density, whereas interactions in the medium infrared with a considerable momentum transfer increase the condensate density, as the loss of condensate is suppressed for lower momenta than the gain.

In figure 4.3, the process of the delay of the transition is further illustrated. Whereas for a higher UV cutoff, the final distribution is close to the original one, for a lower cutoff, the distribution of higher momenta shows a remnant of the original discontinuous distribution of momenta. In fact, the two cascades during the thermalization process have been delayed by the cutoffs. Indeed, during thermalization two processes happen: the distribution spreads out into the UV regions in order to increase entropy, which is compensated by populating soft momenta to ensure energy conservation, including the condensation process. The reason for the effect of the cutoffs is that for high momenta, the maximal momentum transfer lies higher, and by this higher values of the Mandelstam variables are possible, leading to a higher amount of possible interactions being suppressed. More particles

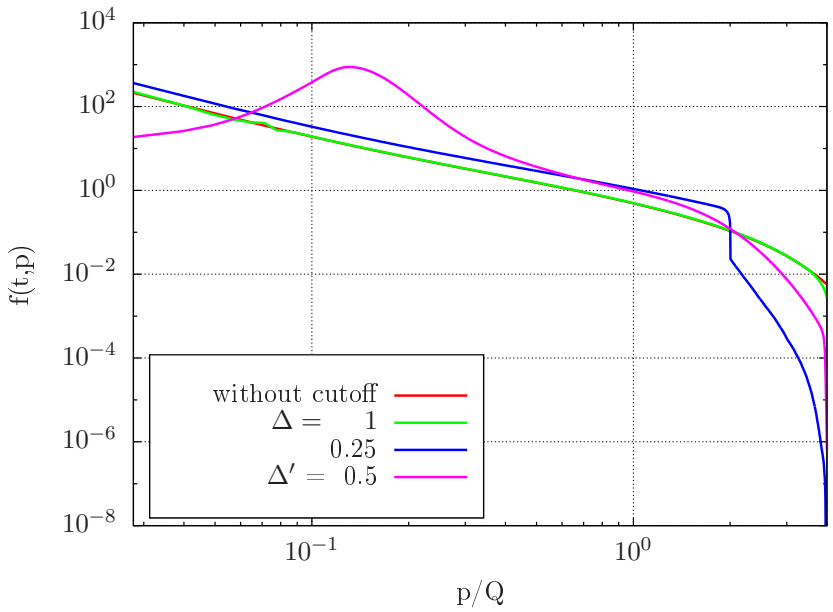

Figure 4.3 – Momentum distribution at $g^4t = 1000$ for a simulation N=1024. Original code from [17] in comparison with modified code for a UV cutoff Δ/IR cutoff Δ' . A CGC-like initial condition was used.

stay in the infrared regime as they cannot progress deeper into the ultraviolet area. With a cutoff in the infrared regime, the opposite effect is observed. One can observe an agglomeration of particles in an intermediate range which would proceed to lower momenta if the interactions would not be suppressed. At the same time, the deep ultraviolet regime is also comparatively underoccupied, as more energy is now present in the area of lower momenta. In fact, the IR cutoff hinders the establishment of the local equilibrium for low momenta. As the occupation number for the CGC initial condition is high for low momenta, there is high scattering rate in this area which creates rapidly an equilibrium in this zone. But these scattering rates are suppressed for an infrared cutoff.

After these illustrative examples, the full power of this generalisation shall be demonstrated by using more common scattering amplitudes.

4.2 Scattering Amplitudes in ϕ^3 and Yang-Mills theory

Scattering amplitudes in massless theories usually contain inverse powers of the Mandelstam variables. If one would use this term directly into the simulation, it would get unstable due to infrared divergences. Indeed, t and u can reach zero. Instead, a regularisation is necessary, at least when higher order corrections are not included in the amplitudes. One may introduce a Debye screening mass, a phenomenon well known from QED by which for example the Coulomb potential of a static charge is modified at great distance. It is derived from the self energy. An approach similar to QED for QCD fails at higher orders due to the non-perturbative behaviour of QCD, however, is very similar in leading order. In fact, the leading order correction can be derived the same way as for QED. This is done by setting $\mu^2 = \lim_{p\to 0} \Pi_L(0,p)$, with $\Pi_{\mu\nu}(p_0,p)$ the self energy of the gluon and Π_L

its longitudinal component (the order of taking the energy and the momentum zero is important). The longitudinal component is taken in analogy to the Coulomb potential, for which the transverse projector does not couple to a static charge. In other words, the Debye screening mass in leading order is the small momentum transfer limit of the longitudinal self-energy, which is equivalent to the scattering off an infinitely heavy, static object. This gives for the gluon the result ([58, 59])

$$\mu^2 = g^2 \frac{N_C T^2}{3} \tag{4.8}$$

for a $SU(N_C)$ Yang-Mills theory in thermal equilibrium at the temperature T, which is derived from the hard thermal loop approximation (HTL) [47]. In this approximation the momenta of the internal particles of the self energy are assumed to be hard, i.e. of order of the temperature or chemical potential, whereas the external momenta are soft, i.e. of the order gT, which is in agreement with the model here. The higher-order corrections would need instead a careful, non-perturbative resummation [60, 61], as the extraction from the electrostatic propagator would be gauge dependent [62]. Nevertheless, for our applications the leading order would be sufficient. It would be now possible to keep track of the Debye mass during the simulation, using the reformulation of the term as applied in [63], which is of the form

$$\mu^2 = \frac{4}{\pi} g^2 \int \frac{d^3\boldsymbol{p}}{(2\pi)^3 \omega_{\boldsymbol{p}}} (N_C f(\boldsymbol{p})). \tag{4.9}$$

The Debye mass acts as a cutoff in the infrared sector and stabilises the calculation. However, this has a drawback. Other than for the gluon pole mass, energy conservation would be not endangered, but the computation could be slowed down. Apart from that, it would be interesting to study how strong the dependence of the screening mass is. Therefore, it will be at this point presented how different choices by hand of the screening mass (in the order of the effective mass, which is the right order for the screening as an approximate calculation showed) affect the outcome of the simulation. From now on, t and u will be changed to $t - \mu^2$ and $u - \mu^2$ as it was done in [63]. The introduction of a Debye mass can be done in a similar way for a Yang-Mills as well as for a ϕ^3 theory, however, the analytic value would be of course different for higher orders.

4.2.1 ϕ^3 theory

In this example, it is assumed that the interaction is governed by an underlying ϕ^3 theory instead of the Yang-Mills-theory of QCD. A $2 \to 2$ interaction is in this model possible via three channels, giving a squared scattering amplitude proportional to

$$g^4 \left[\frac{1}{s} + \frac{1}{t - \mu^2} + \frac{1}{u - \mu^2} \right]^2 \tag{4.10}$$

Taking a look at figure 4.4 shows the strong influence of the screening mass. The values were chosen in the range of what would analytically appear using 4.9. For greater values, it cuts off more infrared contributions, which are crucial for the condensation process with the CGC initial condition, as discussed earlier. Due to this, the transition happens later. Until the transition point is reached, the condensate is loosing more and more particles, as the loss is proportional to the unscreened s-channel as one can see in 4.7. An interesting phenomenon is visible for $\mu^2 = 0.2$, for which the condensate

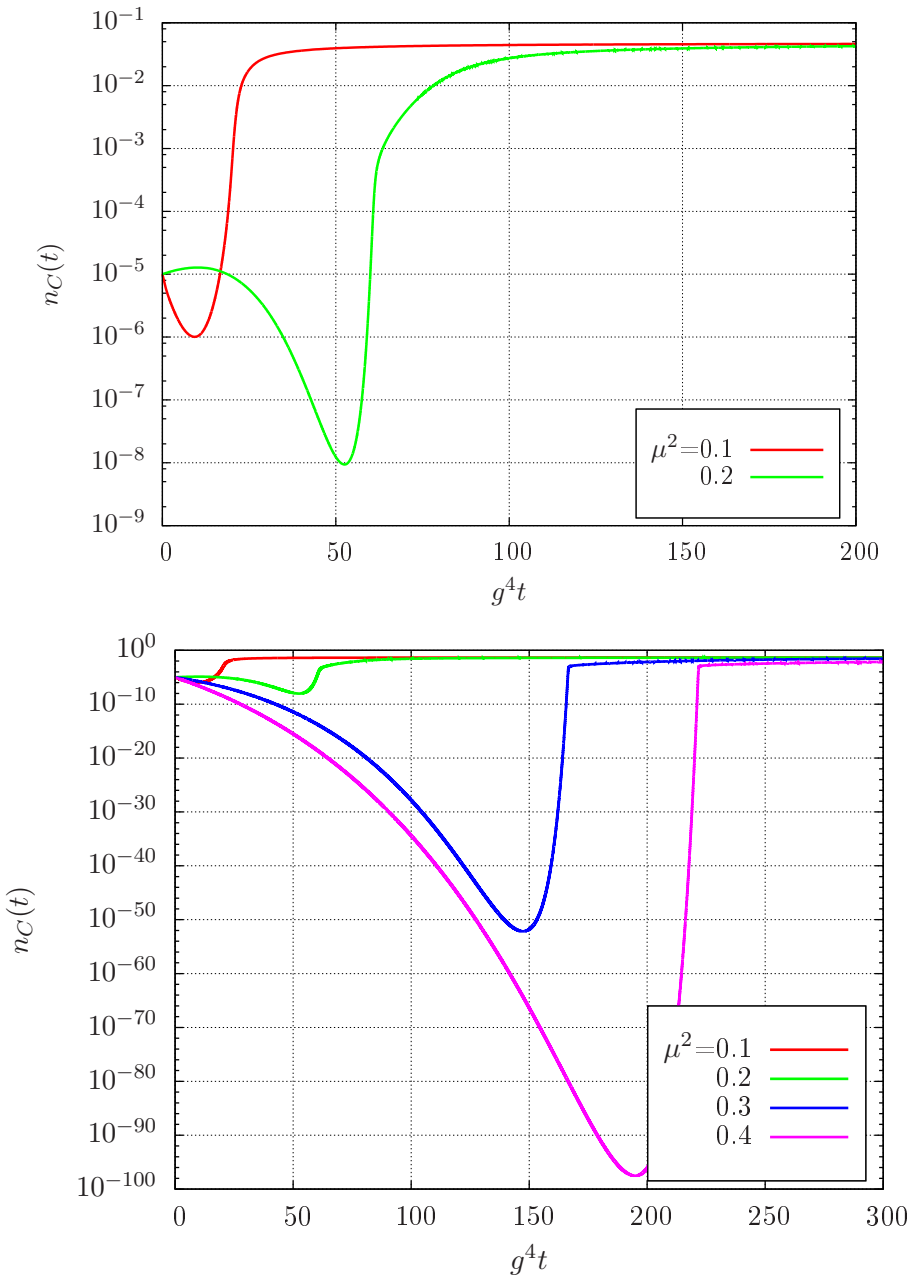

Figure 4.4 – Evolution of the particle density in the condensate in a simulation with N=512 and N_P=12. ϕ^3 amplitude with different values for the Debye screening mass μ^2. The upper figure is is a zoom-in of the figure in the bottom.

density is increasing for a short moment.

Indeed, in figure 4.5 it becomes obvious that for the same initial conditions, the initial slope is highly dependent on the value of the screening mass. Here, instead of the scattering amplitude, its derivative with respect to the screening mass was inserted in the $\partial_t n_C(t)$ integral and the values where compared for different screening masses. As expected, the initial slope has a maximum around a screening mass of 0.18, which matches with the observation in figure 4.4. There is no minimum, as it seems to be constantly falling for $\mu^2 \to \infty$. This example underlines the high importance of the

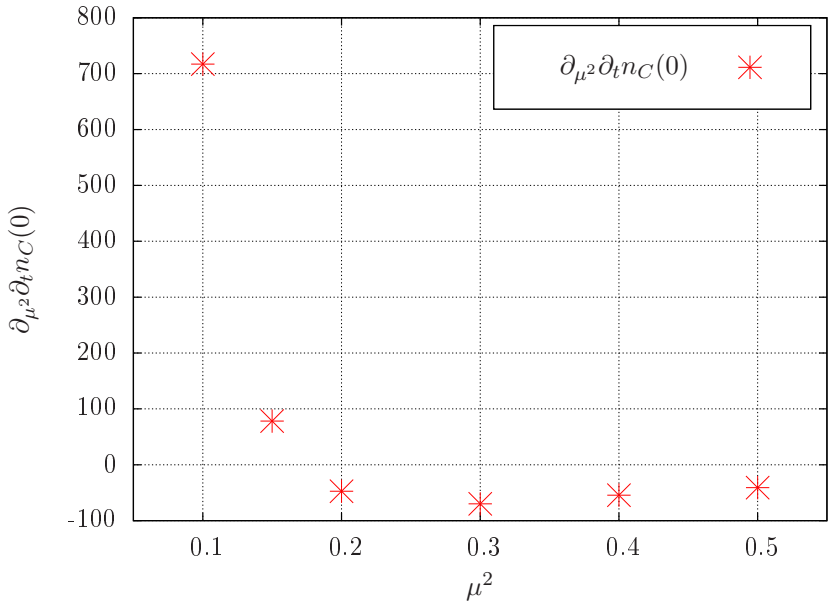

Figure 4.5 – Derivative of the initial slope in the ϕ^3-theory for different values of the screening mass.

correct choice of the Debye screening mass, which has to be known as exactly as possible for a correct qualitatively behaviour at early times, at least for a ϕ^3 interaction. However, for later times, the effect of a change of the screening mass is merely reduced to a speed-up/speed-down, as long as it is not of higher order than t or u.

4.2.2 Yang-Mills theory

A more realistic amplitude for the gluon plasma is the gluon-gluon scattering amplitude, which, up to prefactors, reads in vacuum

$$g^4 \left[3 - \frac{ut}{s^2} - \frac{su}{(t-\mu^2)^2} - \frac{st}{(u-\mu^2)^2} \right] \tag{4.11}$$

where the screening mass was included. Note that s does not need to be regularised, as it is strictly positive. Again, on can take a look at different values of μ. Figure 4.6 shows that the effect of the screening mass is much smaller than for the ϕ^3 amplitude. Indeed, the transition happens very shortly after the start of the simulation. A change of the screening mass only slightly shifts the transition to a later time. This amplitude of a Yang-Mills theory provides a more realistic setup for studying the thermalization process in the CGC than the original ϕ^4 theory used in [17]. Indeed, it would be interesting to investigate the thermalization process with this improved simulation. As explained in the introduction, the speed of the thermalization process, in other words the speed with which the equilibrium state is reached in heavy ion collisions, is an important open question to be explained from QFT. It is therefore a possible approach to compare the timescale with which thermalization happens in the ϕ^4 theory in comparison to the now achieved improvements. However, it is not clear how to compare the timescales of the simulation, since the amplitudes of ϕ^4 and Yang-Mills theories lead to different cross-sections. A possible strategy for comparison which will be used here, is to

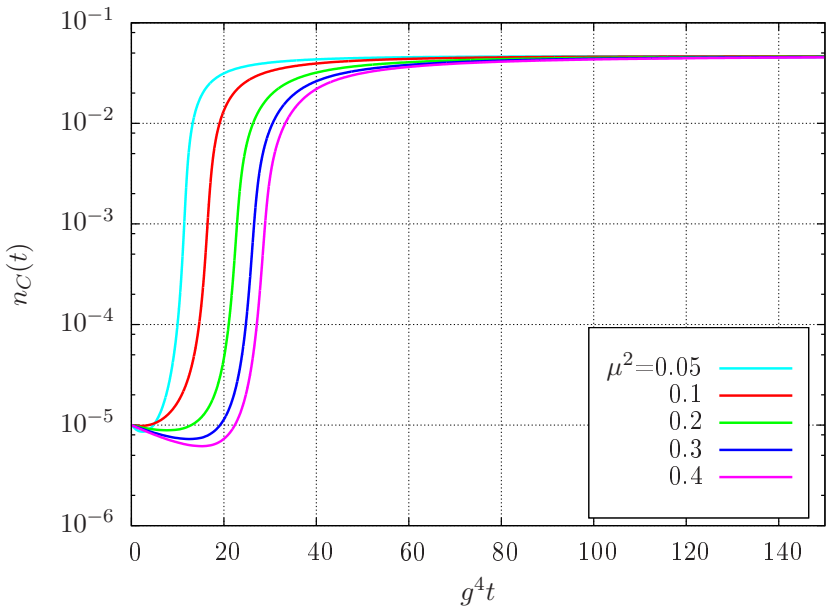

Figure 4.6 – Development of the particle density in the condensate in a simulation with N=512 and N_P=12. Gluon-gluon-scattering amplitude with different values for the Debye screening mass μ^2.

rescale the time so that the rates of variation of the condensate density at $t = 0$ are the same in both theories. This is displayed in 4.7. A Debye mass of 0.1 was chosen.

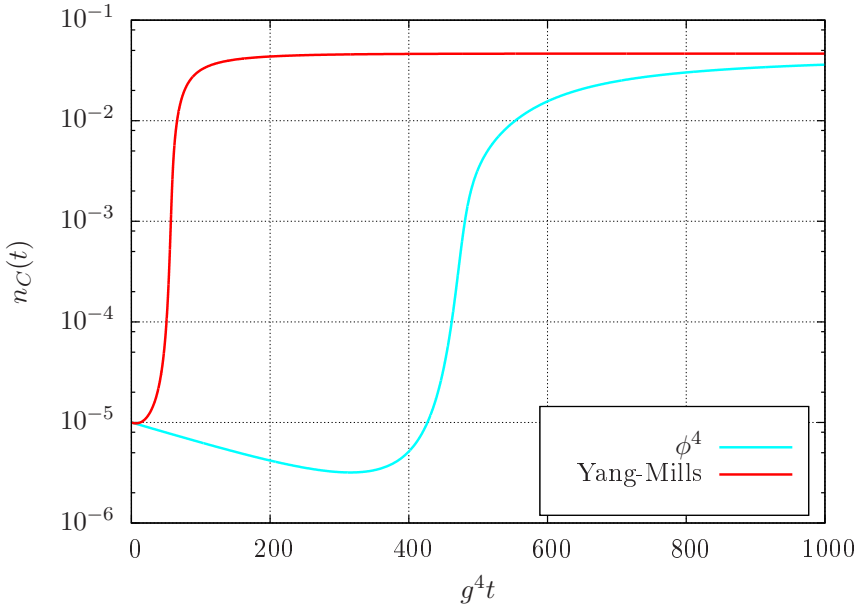

Figure 4.7 – Development of the particle density in the condensate in a simulation with N=512, comparison of speed between gluon-gluon-scattering with $\mu^2 = 0.1$ and the ϕ^4 theory.

It is possible to make two observations. The first is that the transition starts quasi-instantly in Yang-Mills theory in comparison to the ϕ^4 model. Although there is still a loss of condensate in the beginning, it stops around 20 times earlier. Additionally, the transition resembles much more to a discontinuity. Even for long after the transition happened, the condensate is not completely filled for

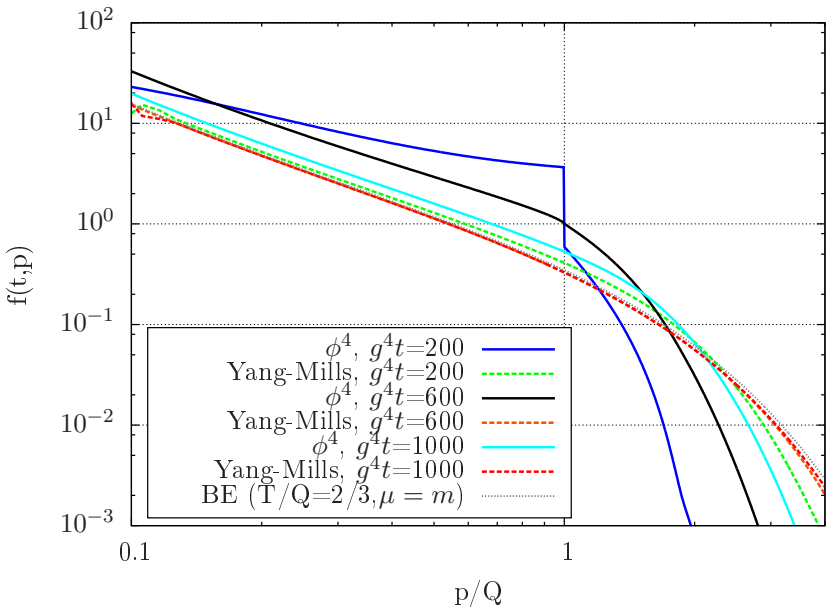

Figure 4.8 – Comparison of the momentum distribution at different points in time in a simulation with N=512 and N_P=12 between gluon-gluon-scattering with $\mu^2 = 0.1$ and the ϕ^4 theory. The grey line is a fit with a Bose-Einstein distribution with chemical potential $\mu = m$.

the ϕ^4 model, and continues to grow for a long time towards the same value as for the Yang-Mills term. On the other hand, for the latter one the condensate density is quasi-static after a short time after leaving the quasi-discontinuous phase. This is a hint that the Yang-Mills term shows the speed up in thermalization which is required to match the hydrodynamical behaviour as outlined in the introduction. Therefore also a look at the momentum distribution is taken.

Figure 4.8 shows the momentum distribution shortly after the transition for the gluon-gluon-scattering, shortly after the transition in the ϕ^4 theory and for late times. One can see that after the transition, the simulation with the Yang-Mills term has basically reached the equilibrium. There are only small changes in the UV region at later times. This is not the case for the ϕ^4 theory, where after the transition the transfer between UV and IR regions is not yet completed and goes on with decreasing speed. However, in comparison with the cutoff behaviour studied earlier, the development for the Yang-Mills-term shows no retarded behaviour in specific momentum regions, but shows the same qualitative behaviour as the ϕ^4 simulation, except some numerical inaccuracies in the deep IR regime. The Yang-Mills term respects the local equilibrium for small momenta as observed before in the ϕ^4 theory. Its main feature is a faster and less smooth condensate transition, which increases the speed of thermalization.

Conclusion

Starting form the results of [17], which explored the thermalization process in kinetic theory with elastic collisions, the simulation was improved. Knowing that kinetic theory is a simpler approach to the problem of thermalization in CGC than for example CSA, it is important to widen range of applicability, as the original algorithm was only applicable to the elastic $2 \to 2$ collision term with scalar ϕ^4 interaction. For this, simplifications of the calculation were needed in order to be able to solve the problem computationally. The approximations done in [17] were carefully revisited and unnecessary assumptions were dropped. Although the runtime of the simulation was considerably increased, it is now possible to include any elastic $2 \to 2$ amplitude which respects the symmetry of the interactions.

The generalisation to reach this was tested for its consistency with the old results both analytically and numerically, where no conflict could be found. Then, several examples of the potential of the new algorithm were presented. Momentum-dependent cutoffs revealed the dependence of the development of the condensate density on almost only the infrared sector for the standard CGC initial conditions. Transition time and condensate density remain almost unchanged as long as the cutoff does not suppress interactions amongst soft particles. In the infrared sector itself, interactions between particles of lower energy are predominantly responsible for a condensate loss, whereas the medium infrared sector is responsible for a gain of condensate particles.

In a second step, the full potential of the code was proven by simulating the $2 \to 2$ scattering process both in the ϕ^3 theory as well as with a gluon-gluon scattering amplitude. Here, the dependency on the choice of the Debye screening mass was demonstrated, which was considerably greater for the ϕ^3 theory. For this, the initial stages compared to ϕ^4 theory shows a qualitatively different behaviour for a certain range of screening masses. For the Yang-Mills interaction, on the other hand, the screening mass only influences the speed of the transition. It was demonstrated that the usage of the gluon-gluon scattering amplitude allows a much faster thermalization process as observed numerically with the ϕ^4 theory. Experimental observations demand a very high speed of of thermalization.

Two parameters of the simulation could in principle be computed instead of set by hand: the mass of the particles as well as their screening mass. It was discussed that the effective mass should not be computed for each timestep, although being time dependent, in order to avoid violations of energy conservation. Instead it could be determined approximately form the final distribution. The screening mass, on the other hand, could be computed at the end of each timestep. This could lead to further improvements of the simulation.

Another possible approach of improvements is of course to include higher-order contributions in the $2 \to 2$ scattering amplitudes. However, the evolution of the Glasma is not necessarily limited to that. Inspired by [51], it would also be interesting to include non-elastic processes. This would relax the particle number conservation and by this could have a strong impact on the condensation process. Another interesting extension would be to drop the assumptions of isotropy or spatial homogeneity, however, this would cause a great loss of computational speed. Most Boltzmann solvers rely on such symmetries. Additionally, it could be tried to include the rapid boost-invariant longitudinal expansion, too.

From the analytical side, it would be interesting to find means in order to determine the point of transition without being dependent on the numerical simulation. By this, it would be possible to predict the timescale of thermalization, as a thermal equilibrium can be only reached after the condensate has been formed. However, finding the for example the inclination point in 2.20 is a difficult task.

Apart from this, it should be also mentioned that the original motivation of studying the thermalization process was the great success of ideal hydrodynamic simulations as pointed out in the introduction. However, there has been no evidence yet that full thermalization or even isotropization is reached [64]. This questions whether hydrodynamic behaviour emerges at the point when full thermalization from the initial conditions is achieved, or at another point in time. This shows that considerable work is still to be done in order to completely understand the thermalization problem for heavy ion collisions.

References

[1] U. W. Heinz, « Early collective expansion: Relativistic hydrodynamics and the transport properties of QCD matter », Landolt-Bornstein **23**, 240 (2010), arXiv:0901.4355 [nucl-th].

[2] S. M. Sanches, D. A. Fogaça and F. S. Navarra, « The time evolution of the quark gluon plasma in the early universe », **630**, 012028 (2015).

[3] U. W. Heinz, « Thermalization at RHIC », AIP Conf. Proc. **739**, 163 (2004), arXiv:nucl-th/0407067 [nucl-th].

[4] L. V. Gribov, E. M. Levin and M. G. Ryskin, « Semihard Processes in QCD », Phys. Rept. **100**, 1 (1983).

[5] R. Baier, A. H. Mueller, D. Schiff and D. T. Son, « 'Bottom up' thermalization in heavy ion collisions », Phys. Lett. **B 502**, 51 (2001), arXiv:hep-ph/0009237 [hep-ph].

[6] Y. V. Kovchegov, « Can thermalization in heavy ion collisions be described by QCD diagrams? », Nucl. Phys. **A 762**, 298 (2005), arXiv:hep-ph/0503038 [hep-ph].

[7] P. M. Chesler and L. G. Yaffe, « Horizon formation and far-from-equilibrium isotropization in supersymmetric Yang-Mills plasma », Phys. Rev. Lett. **102**, 211601 (2009), arXiv:0812.2053 [hep-th].

[8] P. M. Chesler and L. G. Yaffe, « Boost invariant flow, black hole formation, and far-from-equilibrium dynamics in N = 4 supersymmetric Yang-Mills theory », Phys. Rev. **D 82**, 026006 (2010), arXiv:0906.4426 [hep-th].

[9] Y. V. Kovchegov and S. Lin, « Toward Thermalization in Heavy Ion Collisions at Strong Coupling », JHEP **03**, 057 (2010), arXiv:0911.4707 [hep-th].

[10] V. Balasubramanian, A. Bernamonti, J. de Boer, N. Copland, B. Craps, E. Keski-Vakkuri, B. Muller, A. Schafer, M. Shigemori and W. Staessens, « Thermalization of Strongly Coupled Field Theories », Phys. Rev. Lett. **106**, 191601 (2011), arXiv:1012.4753 [hep-th].

[11] E. Iancu and R. Venugopalan, « The Color glass condensate and high-energy scattering in QCD », in *Quark-gluon plasma 4*, edited by R. C. Hwa and X.-N. Wang (2003), 249–3363, arXiv:hep-ph/0303204 [hep-ph].

[12] F. Gelis, E. Iancu, J. Jalilian-Marian and R. Venugopalan, « The Color Glass Condensate », Ann. Rev. Nucl. Part. Sci. **60**, 463 (2010), arXiv:1002.0333 [hep-ph].

[13] K. Fukushima and F. Gelis, « The evolving Glasma », Nucl. Phys. **A 874**, 108 (2012), arXiv:1106.1396 [hep-ph].

[14] K. Fukushima, « Initial fields and instability in the classical model of the heavy-ion collision », Phys. Rev. **C76**, [Erratum: Phys. Rev.C77,029901(2007)], 021902 (2007), arXiv:0711.2634 [hep-ph].

[15] A. H. Mueller and D. T. Son, « On the Equivalence between the Boltzmann equation and classical field theory at large occupation numbers », Phys. Lett. **B 582**, 279 (2004), arXiv:hep-ph/0212198 [hep-ph].

[16] J. Berges, K. Boguslavski, S. Schlichting and R. Venugopalan, « Basin of attraction for turbulent thermalization and the range of validity of classical-statistical simulations », JHEP **1405**, 054 (2014), arXiv:1312.5216 [hep-ph].

[17] T. Epelbaum, F. Gelis, N. Tanji and B. Wu, « Properties of the Boltzmann equation in the classical approximation », Phys. Rev. **D 90**, 125032 (2014), arXiv:1409.0701 [hep-ph].

[18] F. Gelis, « Initial state and thermalization in the Color Glass Condensate framework », Int. J. Mod. Phys. **E 24**, 1530008 (2015), arXiv:1508.07974 [hep-ph].

[19] F. Gelis, R. B. Peschanski, G. Soyez and L. Schoeffel, « Systematics of geometric scaling », Phys. Lett. **B 647**, 376 (2007), arXiv:hep-ph/0610435 [hep-ph].

[20] H. Kowalski, T. Lappi and R. Venugopalan, « Nuclear enhancement of universal dynamics of high parton densities », Phys. Rev. Lett. **100**, 022303 (2008), arXiv:0705.3047 [hep-ph].

[21] L. D. McLerran and R. Venugopalan, « Computing quark and gluon distribution functions for very large nuclei », Phys. Rev. **D 49**, 2233 (1994), arXiv:hep-ph/9309289 [hep-ph].

[22] L. D. McLerran and R. Venugopalan, « Gluon distribution functions for very large nuclei at small transverse momentum », Phys. Rev. **D 49**, 3352 (1994), arXiv:hep-ph/9311205 [hep-ph].

[23] L. D. McLerran and R. Venugopalan, « Green's functions in the color field of a large nucleus », Phys. Rev. **D 50**, 2225 (1994), arXiv:hep-ph/9402335 [hep-ph].

[24] F. Gelis and R. Venugopalan, « Particle production in field theories coupled to strong external sources », Nucl. Phys. **A 776**, 135 (2006), arXiv:hep-ph/0601209 [hep-ph].

[25] J. Schwinger, « Brownian Motion of a Quantum Oscillator », J. Math. Phys. **2**, 407 (1961).

[26] L. Keldysh, « Ionization in the Field of a Strong Electromagnetic Wave », Sov. Phys. JETP **20**, 1307 (1964).

[27] R. E. Cutkosky, « Singularities and discontinuities of feynman amplitudes », J. Math. Phys. **1**, 429 (1960).

[28] A. Ayala, J. Jalilian-Marian, L. D. McLerran and R. Venugopalan, « Quantum corrections to the Weizsacker-Williams gluon distribution function at small x », Phys. Rev. **D 53**, 458 (1996), arXiv:hep-ph/9508302 [hep-ph].

[29] F. Gelis, T. Lappi and R. Venugopalan, « High energy factorization in nucleus-nucleus collisions », Phys. Rev. **D 78**, 054019 (2008), arXiv:0804.2630 [hep-ph].

[30] I. Balitsky, « Operator expansion for high-energy scattering », Nucl. Phys. **B 463**, 99 (1996), arXiv:hep-ph/9509348 [hep-ph].

[31] J. Jalilian-Marian, A. Kovner, A. Leonidov and H. Weigert, « Unitarization of gluon distribution in the doubly logarithmic regime at high density », Phys. Rev. **D 59**, [Erratum: Phys. Rev.D59,099903(1999)], 034007 (1999), arXiv:hep-ph/9807462 [hep-ph].

[32] E. Iancu and L. D. McLerran, « Saturation and universality in QCD at small x », Phys. Lett. **B 510**, 145 (2001), arXiv:hep-ph/0103032 [hep-ph].

[33] E. Ferreiro, E. Iancu, A. Leonidov and L. McLerran, « Nonlinear gluon evolution in the color glass condensate. 2. », Nucl. Phys. **A 703**, 489 (2002), arXiv:hep-ph/0109115 [hep-ph].

[34] P. Romatschke and R. Venugopalan, « The Unstable Glasma », Phys. Rev. **D 74**, 045011 (2006), arXiv:hep-ph/0605045 [hep-ph].

[35] T. Kunihiro, B. Muller, A. Ohnishi, A. Schafer, T. T. Takahashi and A. Yamamoto, « Chaotic behavior in classical Yang-Mills dynamics », Phys. Rev. **D 82**, 114015 (2010), arXiv:1008.1156 [hep-ph].

[36] E. S. Weibel, « Spontaneously growing transverse waves in a plasma due to an anisotropic velocity distribution », Phys. Rev. Lett. **2**, 83 (1959).

[37] S. Mrowczynski, « Instabilities driven equilibration of the quark-gluon plasma », Acta Phys. Polon. **B 37**, 427 (2006), arXiv:hep-ph/0511052 [hep-ph].

[38] A. Kurkela and G. D. Moore, « Bjorken Flow, Plasma Instabilities, and Thermalization », JHEP **1111**, 120 (2011), arXiv:1108.4684 [hep-ph].

[39] A. Dumitru, Y. Nara and M. Strickland, « Ultraviolet avalanche in anisotropic non-Abelian plasmas », Phys. Rev. **D75**, 025016 (2007), arXiv:hep-ph/0604149 [hep-ph].

[40] K. Dusling, T. Epelbaum, F. Gelis and R. Venugopalan, « Role of quantum fluctuations in a system with strong fields: Onset of hydrodynamical flow », Nucl. Phys. **A 850**, 69 (2011), arXiv:1009.4363 [hep-ph].

[41] T. Epelbaum and F. Gelis, « Pressure isotropization in high energy heavy ion collisions », Phys. Rev. Lett. **111**, 232301 (2013), arXiv:1307.2214 [hep-ph].

[42] T. Epelbaum and F. Gelis, « Fluctuations of the initial color fields in high energy heavy ion collisions », Phys. Rev. **D 88**, 085015 (2013), arXiv:1307.1765 [hep-ph].

[43] A. Kurkela and G. D. Moore, « Thermalization in Weakly Coupled Nonabelian Plasmas », JHEP **12**, 044 (2011), arXiv:1107.5050 [hep-ph].

[44] T. Stockamp, « Classical approximation of the Boltzmann equation in high energy QCD », J. Phys. **G 32**, 39 (2006), arXiv:hep-ph/0408206 [hep-ph].

[45] J.-P. Blaizot and E. Iancu, « A Boltzmann equation for the QCD plasma », Nucl. Phys. **B 557**, 183 (1999), arXiv:hep-ph/9903389 [hep-ph].

[46] S. Weinstock, « Boltzmann collision term », Phys. Rev. **D73**, 025005 (2006), arXiv:hep-ph/0510417 [hep-ph].

[47] F. Gelis, *Advanced Topics in Quantum Field Theory* (École Polytechnique, 2019).

[48] S. Jeon, « The Boltzmann equation in classical and quantum field theory », Phys. Rev. **C 72**, 014907 (2005), arXiv:hep-ph/0412121 [hep-ph].

[49] T. Epelbaum, F. Gelis and B. Wu, « Nonrenormalizability of the classical statistical approximation », Phys. Rev. **D 90**, 065029 (2014), arXiv:1402.0115 [hep-ph].

[50] J.-P. Blaizot, J. Liao and L. McLerran, « Gluon Transport Equation in the Small Angle Approximation and the Onset of Bose-Einstein Condensation », Nucl. Phys. **A 920**, 58 (2013), arXiv:1305.2119 [hep-ph].

[51] X.-G. Huang and J. Liao, « Kinetic evolution of the glasma and thermalization in heavy ion collisions », Int. J. Mod. Phys. **E23**, 1430003 (2014), arXiv:1402.5578 [nucl-th].

[52] R. Lacaze, P. Lallemand, Y. Pomeau and S. Rica, « Dynamical formation of a bose–einstein condensate », Physica **D 152**, 779 (2001).

[53] K. Huang, *Statistical Mechanics*, 2nd ed. (John Wiley & Sons, 1987).

[54] J. M. Cornwall, « Dynamical mass generation in continuum quantum chromodynamics », Phys. Rev. **D 26**, 1453 (1982).

[55] J. E. Mandula and M. Ogilvie, « The Gluon Is Massive: A Lattice Calculation of the Gluon Propagator in the Landau Gauge », Phys. Lett. **B185**, 127 (1987).

[56] O. Oliveira and P. Bicudo, « Running Gluon Mass from Landau Gauge Lattice QCD Propagator », J. Phys. **G 38**, 045003 (2011), arXiv:1002.4151 [hep-lat].

[57] D. V. Semikoz and I. I. Tkachev, « Condensation of bosons in kinetic regime », Phys. Rev. **D 55**, 489 (1997), arXiv:hep-ph/9507306 [hep-ph].

[58] J. I. Kapusta and C. Gale, *Finite-temperature field theory: Principles and applications*, Cambridge Monographs on Mathematical Physics (Cambridge University Press, 2011).

[59] D. J. Gross, R. D. Pisarski and L. G. Yaffe, « QCD and instantons at finite temperature », Rev. Mod. Phys. **53**, 43 (1981).

[60] A. K. Rebhan, « The Non-Abelian Debye mass at next-to-leading order », Phys. Rev. **D 48**, 3967 (1993), arXiv:hep-ph/9308232 [hep-ph].

[61] E. Braaten and A. Nieto, « Next-to-leading order Debye mass for the quark - gluon plasma », Phys. Rev. Lett. **73**, 2402 (1994), arXiv:hep-ph/9408273 [hep-ph].

[62] S. Nadkarni, « Non-abelian debye screening: the color-averaged potential », Phys. Rev. **D 33**, 3738 (1986).

[63] M. Greif, F. Senzel, H. Kremer, K. Zhou, C. Greiner and Z. Xu, « Nonequilibrium photon production in partonic transport simulations », Phys. Rev. **C 95**, 054903 (2017), arXiv:1612.05811 [hep-ph].

[64] M. Strickland, « Thermalization and isotropization in heavy-ion collisions », Pramana **84**, 671 (2015), arXiv:1312.2285 [hep-ph].

List of Figures